Ph.D. Thesis

Analysis of baryonic matter in a magnetic field from skyrmion crystal approach

スカーミオン結晶手法を用いた磁場中でのバリオン物質の解析

Mamiya Kawaguchi

川口眞実也

Abstract

Hadrons such as neutrons and protons are the particles which feel the strong force. Although this force is described by the theory of Quantum Chromo-Dynamics (QCD), many parts in low energy region remain uncovered due to the nonperturbative nature of QCD: the mass generation mechanism for nucleon in terms of the chiral symmetry breaking has not completely been clarified yet. Through extreme conditions like the high density, high temperature region and strong magnetic field, the hadron properties would be drastically changed and, as a consequence, one of striking clues would emerge in front of us to reveal the novel aspect for understanding QCD.

To extract a novel insight of the nonperturbative feature for QCD, especially the role of the chiral symmetry, we explore baryonic matter properties in a strong magnetic field based on the skyrmion crystal model. It is found that the magnetic effect plays the role of a catalyzer for the topological phase transition (topological deformation for the skyrmion crystal configuration from the skrymion phase to half-skyrmion phase). We also discuss the magnetic dependence on the inhomogeneity for the chiral condensate in the crystal medium. We find that even in the presence of the magnetic field, the inhomogeneous chiral condensate persists both in the skyrmion and half-skyrmion phases. In particular as the strength of a magnetic field gets larger, the inhomogeneous chiral condensate in the skyrmion phase tends to be drastically localized, while in the half-skyrmion phase the inhomogeneity configuration does not feel a magnetic field at all. We further investigate the magnetic effect on the skyrmion crystal configuration and the single-baryon shape in the crystal medium. It turns out that a strong magnetic field in a low density region (in the skyrmion phase) makes the baryon shape like an elliptic form, while the whole crystal configuration essentially holds. In a high density region (in the half-skyrmion phase), we further observe that a strong magnetic field drastically spoils the crystal structure. A possible correlation between the inhomogeneity of chiral condensate and the deformation of the skyrmion crystal configuration is also addressed. Those findings might be relevant to deepen the understanding for the nonperturbative nature of QCD.

Contents

Chapter 1

Introduction

The quantum chromodynamics (QCD) is well known as the strong interaction theory which describes the quark- and gluon-dynamics. However, many parts of this theory in low energy region have not yet been clarified due to the nonperturbative nature of QCD. Although the major part of nucleon mass has naively been believed to be generated by spontaneous breaking of the chiral symmetry due to the strong QCD interactions, the mass generation mechanism via the chiral symmetry breaking is actually mysterious and has not completely been understood yet.

One key way allowing to tackle this issue is to put the QCD system in high temperature/dense environment or a strong magnetic field: the hadron properties including masses and interactions would be drastically changed. As a consequence, the chiral symmetry could be restored, so that one might deduce how much the chiral symmetry breaking is responsible for the origin of hadron masses. Therefore the QCD phase transition under an extreme environment is a major concern for the strong-interaction physics.

Particularly, looking at a high-baryon number density region, the quantitative and qualitative understanding of QCD has not been clarified yet. Because the high density region involves an intricate theoretical issue, called the sign problem in lattice QCD, so that it is hard to do the straightforward nonperturbative computations. In that sense, it would be the analysis based on the effective models in the high dense environment that is expected to give the novel insight for understanding the QCD phase structure.

Exploring the phase diagram of QCD under an external magnetic field have been extensively studied in high energy physics relevant to the early stage of heavy ion collisions, compact stars, and the early universe (for a recent review see, e.g., Ref. [1]). Of the chiral effective approaches, interesting phenomena would emerge in front of us by considering the magnetic effect on the low energy physics of QCD. Below we shall show some studies on hadron properties under a magnetic field, which are relevant to the chiral dynamics.

In an external magnetic field, for instance, the vector meson gets the nontrivial magnetic dependence, and then the effective mass of vector meson tends to decrease monotonically. In a strong magnetic field region, it would be expected that the superconductivity would show up via vanishing vector-meson mass as discussed in [2, 3, 4, 5, 6, 7, 8].

What's more, a magnetic field derives the significant mixing among mesons through analyzing the chiral perturbation theory with the hidden local symmetry [9, 10]. Particularly, it leads to the dramatic enhancement for the omega meson mass, this observable is testable by the lattice QCD [8]. These findings based on effective model approaches provide the motivation for the lattice simulation.

Furthermore, a magnetic field makes hadrons long-lived. As for the decay width of neutral rho meson, it is naively expected that the neutral rho meson would be long-lived in a magnetic field due to the magnetic enhancement on the charged pion mass. However, by computing directly the charged pion loop correction to the neutral rho meson propagator, it turns out that the decay properties of the neutral rho meson become more complicated and the lifetime deviates from the naive expectation [11, 12].

Of particular interest among what is anticipated is that the spontaneous chiral symmetry breaking is affected by the magnetic effect. Some studies show that a magnetic field plays the role of catalyzer or inverse catalyzer for the chiral symmetry breaking through the analysis of various effective theories, i.e. the chiral perturbation theory [13, 14, 15, 16] and Nambu-Jona-Lasinio model [17, 18, 19, 20, 21].

Incidentally, even in a high temperature region, the characteristical phenomena in correlation with an intrinsic magnetic property of hadrons emerge, called the chiral magnetic effect [23, 24, 25]. This magnetic effect is actually closely tied with the topological vacuum structure of QCD and the critical issue on the (charge-conjugate (C) and) parity (P) breaking in QCD, so having attracted a great attention so far. In particular, it would be expected that the local parity-odd domain would show up in a short-time scale of the hot QCD system, hence could be crated by heavy ion collisions (for a review, see [22]). This local domain is called the chiral imbalance medium, which can be regarded as the time variation of the strong CP phase [23, 24, 25, 26, 27] locally dictating the chiral asymmetry through the chiral anomaly equation. Actually, the chiral-imbalance medium induces CP-odd interactions between pions and a photon, a magnetic field in part, so that the electromagnetic form factor of charged pions gets the the parity breaking effect [28]. Consequently, the emergence of this parity-odd form factor is phenomenologically reflected in the elastic scattering of a pion and a photon in the chiral imbalance medium, which might be in experiments contaminated with the events associated with the chiral magnetic effect. By specifying the polarization for the photon associated with the charged pion emission, the asymmetry rate of the parity violation is quantified and a typical size of the asymmetry

is roughly estimated. Thus, it is theoretically demonstrated that the asymmetry signal is large enough over the expected background events in heavy ion collision experiments, hence the signal could be sufficient to detect the remnant of the strong CP violation.

Thus the magnetic field has a powerful probe to extract a new aspect of the chiral symmetry breaking and its related hadron properties. In this thesis, we attempt to extract such a new aspect from a baryonic matter set on a magnetic field, based on the Skyrme model.

The Skyrme model is a chiral effective theory based on the nonlinear realization of the chiral symmetry and built in a limit with a large number of colors (large N_c), which deals with baryon properties such as the baryon mass and baryons interaction. What should be noted is that in this framework the baryon is identified as the topologically static-object which is the so-called skyrmion [29]. Actually, the large-N_c QCD supports that the topologically-static soliton arising as a solution of Skyrme model can be regarded as the baryon [30, 31]. Since this is merely a model based on model based on the ideal large N_c, not a real-life QCD with Nc=3, quantitative arguments such as fitting to experimental data may not be reliable. However, we can expect that underlying properties of baryon should qualitatively be extracted through analyzing the skyrmion, because the Skyrme model has the essential features of QCD, i.e. the chiral symmetry and the large-N_c concept.

Intriguingly, the skyrmion approach can be extended to the infinite baryonic matter [32]. This baryonic matter is called the skyrmion crystal, and can be a most powerful approach for the baryon description in high density region, where baryons can look like a static and highly compressed object, as if they could form crystals. In the skyrmion crystal approach, we can thus observe the baryonic matter structure, the medium dependence of hadron properties and the chiral restoration phenomenon[33, 34, 35, 36, 37]. Of particular interest is to note that the skyrmion crystal approach has a characteristic phenomena. In the high-density skyrmion crystal, the skyrmion configuration changes to be another structure form. This phenomenon is the topological phase transition for the skyrmion crystal configuration. If we choose the underlying structure as the face-centered-cubic (FCC) crystal, the crystal configuration is changed from a face-centered-cubic skyrmion crystal to a cubic-centered half-skyrmion crystal. The findings in the skyrmion crystal approach might deepen our understanding of a high dense matter.

In this thesis, we shall turn on the external magnetic field for such a skyrmion crystal configuration, to analyze the magnetic properties of a baryonic matter based on the skyrmion crystal model, especially the FCC crystal chosen. We observe that the energy of the skyrmion crystal gets larger as the strength of a magnetic field increases. It is also found that a magnetic

field acts as the catalyzer for the topological phase transition. Paying a particular attention into the inhomogeneity of the chiral condensate in the baryonic matter, it turns out that the underlying inhomogeneous distribution of chiral condensate keeps for any density region even in the presence of a magnetic field. Of particular interest among our findings is that the skyrmion crystal configuration and the single-baryon shape in the crystal are distorted by a magnetic field. In a low density region the single-baryon shape is deformed to be an elliptic form, however, the intrinsic crystal structure persists. On the other hand, in a high density region, it is further found that the skyrmion crystal is drastically disfigured out of the intrinsic crystal structure.

What we find in this study might deepen our understanding of a high dense matter and reveal the new aspect of the nonperturbative feature for QCD.

This thesis is organized as follows: in Chap.2, we introduce a basic idea on the model building in hadron physics via the spontaneous chiral symmetry breaking. Then, we briefly review the Skyrme model in Chap.3, which describes the baryon (skyrmion) and baryonic matter (skyrmion crystal) properties. With these setups for studying the baryonic matter and introducing a magnetic field, we analyze the magnetic properties of the skyrmion crystal, and then we show the numerical results and analyze some phenomena related to the chiral symmetry in Chap.4. Conclusion for this thesis is given in Chap.5, and we make comments on the application of the skyrmion crystal approach to other interesting phenomena in a baryonic matter.

Chapter 2

QCD and spontaneous chiral symmetry breaking

QCD is the strong interaction theory and the fundamental theory of hadron dynamics. Of interest is that QCD has some symmetries. For instance, in the massless limit of up- and down-quarks QCD Lagrangian is invariant under the chiral symmetry, $SU(2)_L \times SU(2)_R$. Looking at the low energy physics, the experimental results in the hadron physics suggest that the chiral symmetry is broken down to $SU(2)_V$. In terms of the Nambu-Goldstone theorem, the massless particles, which is to be identified as pions after getting the small mass by a couple of small explicit-breaking effects, appear via the spontaneous chiral symmetry breaking. Actually, the mechanism based on the spontaneous chiral symmetry breaking has well succeeded in describing the pion dynamics. Thus, to understand the non-perturbative properties of QCD in the low energy region, some models should be provided based on the chiral symmetry, such as the linear σ model and the non-linear σ model.

In this chapter, we start from the QCD Lagrangian and then explain the spontaneous chiral symmetry breaking. Finally, the (non) linear-σ model based on the chiral symmetry is discussed.

2.1 QCD Lagrangian and chiral symmetry

The QCD Lagrangian based on the SU(3) gauge invariance takes the form

$$\mathcal{L}_{\rm QCD} = \sum_f \bar{q}^f (i\gamma^\mu D_\mu - m_f) q^f - \frac{1}{2}\sum_{a=1}^{8} {\rm tr}[(F^a_{\mu\nu}T^a)^2], \tag{2.1}$$

where q_f is the quark field with the flavor index f and $F^a_{\mu\nu}$ represents the field strength of gluon fields,

$$F^a_{\mu\nu}T^a = \partial_\mu A^a_\nu T^a - \partial_\nu A^a_\mu T^a - ig[A^a_\mu T^a, A^b_\nu T^b], \tag{2.2}$$

with A_μ^a being the gluon fields, T^a denoting the generator of $SU(3)$ and g representing the coupling constant. In Eq.(2.1), the covariant derivative of quark fields q reads

$$D_\mu q_f = (\partial_\mu - igA_\mu^a T^a) q_f. \tag{2.3}$$

Now we introduce the projection operator, $P_{R,L}$, to decompose the quark fields into the left- and right-handed components,

$$\begin{aligned} q_R^f &= P_R q^f, \quad q_L^f = P_L q^f, \\ P_{R,L} &= \frac{1 \pm \gamma_5}{2}. \end{aligned} \tag{2.4}$$

By using this projection operator the QCD Lagrangian is rewritten by the left- and right-handed quarks,

$$\begin{aligned} \mathcal{L}_{\rm QCD} &= \sum_f \left(\bar{q}_L^f i\gamma^\mu D_\mu q_L^f + \bar{q}_R^f i\gamma^\mu D_\mu q_R^f \right) - \sum_f m_f \left(\bar{q}_R^f q_L + \bar{q}_L^f q_R \right) \\ &\quad -\frac{1}{2} \sum_{a=1}^{8} {\rm tr}[(F_{\mu\nu}^a T^a)^2]. \end{aligned} \tag{2.5}$$

In the low-energy region relevant to the nuclear physics, the current masses of the u- and d-quarks (m_u, m_d) are much smaller than the typical energy scale of hadron, $\mathcal{O}(1\,{\rm GeV})$, so that the current quark masses is negligible. In the case of the massless quarks, the QCD Lagrangian is invariant under the chiral transformation,

$$q_L \to g_L q_L, \quad q_R \to g_R q_R, \tag{2.6}$$

with $g_{L,R} \in U(N_f)_{L,R}$. The massless QCD has the $U(N_f)_L \times U(N_f)_R$ symmetry which is the so-called chiral symmetry.

2.2 Spontaneous chiral symmetry breaking

The pions, which are the lightest mesons in the hadron physics, play an important role in the hadron dynamics. From the viewpoint of the chiral symmetry, pions can be introduced as Nambu-Goldstone modes (massless particles) via the spontaneous breaking of the chiral symmetry , and the notion of the chiral symmetry breaking successfully captures the appropriate picture to describe the pion dynamics. In this section we briefly explain the spontaneous chiral symmetry breaking.

We consider a general case where the charge Q^a is associated with the Noether current j_μ^a of the symmetry G. Local operators, $\Phi(x)$ are infinitesimally transformed (by $\delta^a \Phi(x)$) under the Noether's charge $Q^a \equiv \int d^3 j_{\mu 0}^a(x)$ as

$$[iQ^a, \Phi(y)] = \delta^a \Phi(y). \tag{2.7}$$

Taking the vacuum expectation value for both sides, we have

$$\langle 0|[iQ^a, \Phi(0)]|0\rangle = i\int d^4x\partial_\mu\langle 0|Tj^{a\mu}(x)\Phi(y)|0\rangle = \langle 0|\delta^a\Phi(y)|0\rangle. \tag{2.8}$$

Inserting the following completeness relation with the complete set $\{|0\rangle, |\lambda_p\rangle\}$ (the latter being having the three-momentum $\mathbf{p}$ and the energy $E_{\mathbf{p}}$ and some quantum number b),

$$\mathbf{1} = |0\rangle\langle 0| + \sum_{\lambda,b}\int \frac{d^3p}{(2\pi)^3}\frac{1}{2E_{\boldsymbol{p}}(\lambda)}|\lambda^b_{\boldsymbol{p}}\rangle\langle\lambda^b_{\boldsymbol{p}}|, \tag{2.9}$$

into Eq.(2.8), we have

$$\begin{aligned}
&i\int d^4x\partial_\mu\langle 0|Tj^{a\mu}(x)\Phi^b(0)|0\rangle \\
&= \int d^4x\sum_{\lambda,b}\int_0^\infty dM^2\delta(M^2-m_\lambda^2)A(\lambda)B(\lambda)\delta^{ab}\int\frac{d^4q}{(2\pi)^4}\frac{q^2}{q^2-M^2}e^{-iq\cdot x} \\
&\begin{cases} = 0, & (M\neq 0) \\ \neq 0, & (M=0), \end{cases}
\end{aligned} \tag{2.10}$$

where $A(\lambda)$ and $B(\lambda)$ have been introduced as

$$\begin{aligned}
\langle 0|j^a_\mu(x)|\lambda^b_{\boldsymbol{p}}\rangle &= -ip_\mu\delta^{ab}A(\lambda)e^{-ip\cdot x}|_{p^0=E_{\boldsymbol{p}}} \\
\langle 0|\Phi^a|\lambda^b_{\boldsymbol{p}}\rangle &= \delta^{ab}B(\lambda)e^{-ip\cdot x}|_{p^0=E_{\boldsymbol{p}}}.
\end{aligned} \tag{2.11}$$

Eq.(2.10) implies that massless particles appear necessarily as the order parameter, $\langle 0|\delta^a\Phi(y)|0\rangle$, gets the nonzero value. Those massless particles are called Nambu-Goldstone bosons (NG bosons). In Eq.(2.10), the NG fields corresponds to the Φ fields. Furthermore, when $\langle 0|\delta^a\Phi(y)|0\rangle \neq 0$, Eq.(2.8) implies that the charge Q related to the symmetry G satisfies the following condition,

$$Q|0\rangle \neq 0. \tag{2.12}$$

This show that after the order parameter $\langle 0|\delta^a\Phi(y)|0\rangle$ gets the nonzero value, the charge Q becomes an ill-defined operator, so the G symmetry no longer is a symmetry at the vacuum $|0\rangle$, and is broken spontaneously. This is called the spontaneous symmetry breaking.

We consider the case of the spontaneous chiral symmetry breaking. The vector- and axial-current are given as

$$j^i_{V\mu} = j^i_{R\mu} + j^i_{L\mu} = \bar{q}\gamma_\mu\tau^i q, \quad j^i_{A\mu} = j^i_{R\mu} - j^i_{L\mu} = \bar{q}\gamma_\mu\gamma_5\tau^i q, \tag{2.13}$$

where $j^i_{L,R}$ (labeled by $i = 1, \cdots, N_f$) is the current associated with the $SU(N_f)_{L,R}$. The corresponding Noether's charges are defined in the same

way as the generic charge introduced as above. We can also introduce the scalar and pseudoscalar operators out of the quark field bilinears,

$$S = \bar{q}q, \quad P^i = \bar{q}i\gamma_5\tau^i q. \tag{2.14}$$

As for the chiral $SU(2)_L \times SU(2)_R$ symmetry, we then have the following relation for the scalar and pseudoscalar currents:

$$i\int d^3x\langle 0|\left[j^i_{A\mu=0}(x), P^k(y)\right]|0\rangle = 2\delta^{ik}\langle 0|S(y)|0\rangle. \tag{2.15}$$

If the quark condensate $\langle 0|\bar{q}q|0\rangle$ gets the nonzero value, the $SU(2)_L \times SU(2)_R$, is spontaneously broken to $SU(2)_V$ via the appearance of Nambu-Goldstone bosons corresponding to the pseudscalar field P^i. Then, one can easily check that for the QCD vacuum $|0\rangle$, the vector charge Q^i_V is the well-defined operator, but the axial-charge Q^i_A is not the well-defined operator:

$$Q^i_V|0\rangle = 0, \quad Q^i_A|0\rangle \neq 0. \tag{2.16}$$

2.3 Non-linear σ model

In a low energy dynamics where pions dominate, the light mesons should be incorporated into the effective model based on the chiral symmetry. In this section, we introduce typical models with respect to the spontaneous chiral symmetry breaking.

To describe the meson field as the quark-antiquark bound state, we introduce the matrix M out of left- and right-handed quark fields

$$M_{ab} = \bar{q}_{Rb}q_{La}, \tag{2.17}$$

with a, b being the flavor indices. The matrix M transforms under the chiral transformations $SU(2)_L \times SU(2)_R$ as

$$M \to g_L M g_R^\dagger. \tag{2.18}$$

Taking trace products in the following way, we can extract the linear combination of quarks,

$$\begin{aligned}
\Phi_i &= \mathrm{tr}[M\tau^i] = \bar{q}_L\tau^i q_R \\
&= \frac{1}{2}\bar{q}\tau^i q + \frac{1}{2}\bar{q}\gamma_5\tau^i q \\
\Phi^{(S)} &= \mathrm{tr}[M] = \bar{q}_L q_R \\
&= \frac{1}{2}\bar{q}q + \frac{1}{2}\bar{q}\gamma_5 q.
\end{aligned} \tag{2.19}$$

Let $g_{L,R}$ be the transformation matrices associated to the vector and axial-vector transformation,

$$g_R = \exp\left[i(\theta^a_V + \theta^a_A)\tau^a\right], \quad g_L = \exp\left[i(\theta^a_V - \theta^a_A)\tau^a\right]. \tag{2.20}$$

When picking up $\bar{q}q$ and $i\bar{q}\gamma_5\tau^i q$ from Eq.(2.19), one can find that under the infinitesimal vector transformation, $\theta_V^a \neq 0, \quad \theta_A^a = 0$, these bilinears transform as

$$\begin{aligned} &\bar{q}q \to \bar{q}q, \\ &i\bar{q}\gamma_5\tau^i q \to i\bar{q}\gamma_5\tau^i q - 2if^{ijk}\theta_V^j \bar{q}\gamma_5\tau^k q. \end{aligned} \tag{2.21}$$

In a similar way, under the infinitesimal axial-vector transformation, $\theta_V^a = 0, \quad \theta_A^a \neq 0$, these bilinears transform as

$$\begin{aligned} &\bar{q}q \to \bar{q}q + 2i\theta_A^i \bar{q}\gamma_5\tau^i q \ , \\ &i\bar{q}\gamma_5\tau^i q \to i\bar{q}\gamma_5\tau^i q - 2\theta_A^i \bar{q}q. \end{aligned} \tag{2.22}$$

Eqs.(2.21) and (2.22) show that $(\bar{q}q)^2 + (i\bar{q}\gamma_5\tau^i q)^2$ is invariant under the chiral transformation.

In the low energy region, the bilinear products, $\bar{q}q$ and $i\bar{q}\gamma_5\tau^i q$, are described as the isosinglet meson field σ and isotriplet-pseudoscalar meson field π^i respectively:

$$\bar{q}q \sim \sigma, \qquad i\bar{q}\gamma_5\tau^i q \sim \pi^i. \tag{2.23}$$

In the chiral invariant way, we can introduce the σ and π^i fields in the matrix M as follows,

$$M = \sigma \mathbf{1}_{2\times 2} + i\tau^i \pi^i. \tag{2.24}$$

By using this matrix M, one can write the chiral invariant Lagrangian,

$$\mathcal{L}_{L\sigma M} = \frac{1}{4}\mathrm{tr}[\partial_\mu M \partial^\mu M^\dagger] - V(M, M^\dagger). \tag{2.25}$$

This Lagrangian constructed out of the matrix M is the so-called linear σ model which is one of the chiral effective models [38, 39].

From the Lagrangian in Eq. (2.25), one can derive the conserved Noether current associated with the chiral $SU(2)_L \times SU(2)_R$ symmetry,

$$\begin{aligned} j^i_{L,\mu} &= \frac{1}{2}\left(f^{ijk}\pi^j \partial_\mu \pi^k - \sigma\partial_\mu \pi^i + \pi^i \partial_\mu \sigma\right) \\ j^i_{R,\mu} &= \frac{1}{2}\left(f^{ijk}\pi^j \partial_\mu \pi^k + \sigma\partial_\mu \pi^i - \pi^i \partial_\mu \sigma\right). \end{aligned} \tag{2.26}$$

The axialvector current and vector current are reconstructed by $j^i_{L(R)\,\mu}$, and read

$$\begin{aligned} j^i_{V\mu} &= J^i_{R,\mu} + J^i_{L,\mu} = f^{ijk}\pi^j \partial_\mu \pi^k \\ j^i_{A\mu} &= J^i_{R,\mu} - J^i_{L,\mu} = \sigma\partial_\mu \pi^i - \pi^i \partial_\mu \sigma. \end{aligned} \tag{2.27}$$

As the chiral symmetry is spontaneously broken at the vacuum state in QCD, the matrix element for $j^a_{A\mu}$ sandwiched by the vacuum and and an on-shell pion state with the momentum p can be denoted as

$$\langle 0|j^a_{A\mu}|\pi^b(p)\rangle = if_\pi p_\mu e^{ip\cdot x}\delta^{ab}, \tag{2.28}$$

where f_π is the pion decay constant.

For the linear sigma model in Eq.(2.25), we shall give a simple potential form to study the analysis of the spontaneous chiral symmetry breaking at the classical field level in terms of the meson field dynamics,

$$V(M, M^\dagger) = -\frac{1}{4}\mu^2 \mathrm{tr}[MM^\dagger] + \lambda \mathrm{tr}(\mathrm{tr}[MM^\dagger])^2, \tag{2.29}$$

where μ^2 and λ are positive parameters. One can easily see that the vacuum expectation value of the sigma field σ gets a nonzero constant value, leading to the spontaneous breaking of the chiral $SU(2)_L \times SU(2)_L$ symmetry, hence the NG bosons (pions) appear. This can be rephrased as

$$\langle 0|j^a_{A\mu}|\pi^b(p)\rangle = \langle 0|(\sigma\partial_\mu\pi^a - \pi^a\partial_\mu\sigma)|\pi^b(p)\rangle = i\langle 0|\sigma|0\rangle p_\mu e^{ip\cdot x}\delta^{ab}. \tag{2.30}$$

From Eqs.(2.30) and (2.28), the vacuum expectation value of the σ field is related to the pion decay constant,

$$f_\pi = \langle 0|\sigma|0\rangle. \tag{2.31}$$

The potential term of linear sigma model is the function of $\sigma^2 + \pi^2$: $V(M, M^\dagger) = V(\sigma^2 + \pi^2)$. As mentioned above, after the chiral symmetry breaking the minimum potential energy should be realized with the constraint condition, $c^2 = \sigma^2 + \pi^2$. Namely, by choosing the nonzero value of $c^2 = \sigma^2 + \pi^2$, the spontaneously symmetry breaking would be realized, e.g. $\sigma = c$ and $\pi = 0$. From the fact in Eq.(2.31), the constant, c, can be generally read as f_π:

$$\sigma^2 + \pi^2 = f_\pi^2. \tag{2.32}$$

In the low-energy region where the sigma field is supposed to be heavy enough to be integrated out, the chiral effective model is described by only the Nambu-Goldstone bosons corresponding to pions. To integrate out the sigma field in the linear sigma model we insert Eq.(2.32) into the matrix M Eq.(2.24) to be

$$M = f_\pi \left[\sqrt{1 - \frac{\pi^2}{f_\pi^2}}\mathbf{1}_{2\times 2} + i\frac{\tau^i\pi^i}{f_\pi}\right]. \tag{2.33}$$

Introducing the new field ϕ_i associated to π_i,

$$\frac{\tau_i\pi_i}{f_\pi} = \sin\left(\frac{\tau_i\phi_i}{f_\pi}\right) \tag{2.34}$$

the matrix M read

$$\begin{aligned} M &= f_\pi \exp\left(\frac{\tau_i \phi_i}{f_\pi}\right) \\ &\equiv f_\pi U. \end{aligned} \tag{2.35}$$

We have introduced the chiral field, U. Now, the matrix M is described by only the ϕ_i which are the redefined-pion fields in a way as in Eq.(2.34). By using the chiral field U, the kinetic term of the linear sigma model can be rewritten as

$$\mathcal{L}^{(\mathrm{kin})}_{L\sigma M} = \frac{1}{4}\mathrm{tr}[\partial_\mu M \partial^\mu M^\dagger] = \frac{f_\pi^2}{4}\mathrm{tr}\left[\partial_\mu U \partial^\mu U^\dagger\right]. \tag{2.36}$$

This Lagrangian composed of the chiral field U is the so-called nonlinear sigma model due to the chiral field U reflecting the nonlinear transformation law for the redefined-pion fields ϕ_i (for the detail of the nonlinear realization, see Appendix A).

Chapter 3

Skyrme model

Before QCD was established as the underlying dynamics for hadrons, Skyrme had proposed, based on the non-linear sigma model, the non-strange baryons are considered as stable soliton configurations with a non-trivial geometrical structure [29]. This stable soliton is called skyrmion. Until quarks forming baryons had come to light, his formidable work was not seriously taken. However, the situation has drastically changed by Witten's argument in which the skyrmion can be identified as the baryon in large-N_c limit [30, 31].

Thinking of a realistic number of colors, $N_c = 3$, one may say that quantitative results for the skyrmion cannot being in agreement with experimental results. It should however be remarked that whole concept for the skyrmion picture is based on the essential features inherit to QCD, such as the chiral symmetry and the large-N_c, so that it should be certainly expected that underlying properties of the baryon structure and intrinsic interactions should qualitatively be reflected.

This chapter introduces such a remarkable features of the Skyrme model (for more on this, see comprehensive reviews [40, 41]).

3.1 Baryon and topology

The chiral field involves a non-trivial topological configuration, hence the nonlinear-σ model has a stable-soliton solution. In Skyrme's idea, this stable soliton can be identified as a baryon. In this section we briefly introduce a stable-baryon configuration from the concept of topology within the framework of the nonlinear-σ model.

As stated in Sec. 2.3, the chiral field U is expressed as

$$U = \exp\left[i\frac{\pi^a\tau^a}{f_\pi}\right], \tag{3.1}$$

where this π^i $(i = 1, 2, 3)$ are the pion field in the nonlinear representation. We assume that the chiral field has the time-independent configuration,

$U(\vec{x})$. For the energy of the stable and static soliton to be finite, the chiral field $U(\vec{x})$ should approach a constant value as $\vec{x} \to \infty$. Thus, when mapping the three-dimensional space onto the isospin space, we should compactify the three dimensional space: the nontrivial map for static configuration, $U(\vec{x})$, is described as

$$U(\vec{x}) : R^3 \to S^3. \tag{3.2}$$

In a low-energy limit, the effective theory based on QCD should go to the vacuum realized by the spontaneous chiral symmetry breaking, $\langle 0|\sigma|0\rangle = f_\pi$. This fact gives us the following boundary condition for the linear sigma model field M and the chiral field U:

$$\lim_{|\vec{x}|\to\infty} \langle 0|M(\vec{x})|0\rangle = f_\pi, \quad U(|\vec{x}| \to \infty) = 1. \tag{3.3}$$

Actually this condition insures that the energy of the topological object is finite. In the concept of the topology, this mapping $U(\vec{x})$ can be viewed as the third homotopy group,

$$\pi_3\left(SU(2)\right) = Z \tag{3.4}$$

where Z is the additive group of integers. These integers are the winding numbers characterized by integer that counts how many times S_3 for the isospin space is wrapped when the three-dimensional spacial coordinate is covered just once. The winding number is associated with the topological current which is given as

$$j^\mu_W \;=\; \frac{1}{24\pi^2}\epsilon^{\mu\nu\rho\sigma}\mathrm{tr}\left[(\partial_\nu U\cdot U^\dagger)(\partial_\rho U\cdot U^\dagger)(\partial_\sigma U\cdot U^\dagger)\right]. \tag{3.5}$$

In the chiral effective theory, the topological current can be derived from the functional derivative of the Wess-Zumino-Witten(WZW) action (for the explicit form, see in Appendix D), $\Gamma_{WZW} = \int d^4x \mathcal{L}_{WZW}$, with the external gauge field of the $U(1)_V$, $\mathcal{V}_{B\mu}$:

$$j^\mu_W \;=\; \left.\frac{\partial\Gamma_{WZW}}{\partial\mathcal{V}_{B\mu}}\right|_{\mathcal{V}_{B\mu}\to 0}. \tag{3.6}$$

This means that the topological current can be identified as the baryon current j^μ_B,

$$j^\mu_B = j^\mu_W. \tag{3.7}$$

The winding number (the baryon number) B thus takes the form,

$$B = \int d^3x j^0_W. \tag{3.8}$$

It is naturally expected that the topologically nontrivial soliton with $B = 1$ corresponds to the baryon. Note that the winding number is only characterized by the boundary condition of $U(\vec{x})$. Assuming that this boundary condition keeps even when time continuously evolves, hence the winding numbers are conserved fully in a real space-time, so that the topological solution is the static object.

3.2 Skyrmion

With the above concept, we are now ready to explain the skyrmion properties such as the energy and the charge radius of the skyrmion through employing the Skyrme model which is based on the nonlinear sigma model. Here, we briefly review the Skyrme model.

The Skyrme model [29] in the chiral limit, based on the 2-flavor chiral symmetry, is given as

$$\mathcal{L}_{\rm Skyr} = \frac{f_\pi^2}{4}{\rm tr}[\partial_\mu U \partial^\mu U^\dagger] + \frac{1}{32g^2}{\rm tr}\Big([U^\dagger\partial_\mu U, U^\dagger\partial_\nu U][U^\dagger\partial^\mu U, U^\dagger\partial^\nu U]\Big), \quad (3.9)$$

where g is the dimensionless coupling constant. The second term is the so-called Skyrme term which is introduced to stabilize the static soliton to have the finite-energy. To study the baryon physics based on the soliton picture, Skyrme proposed an appropriate ansatz for the soliton configuration like

$$U(\boldsymbol{x}) \;=\; \exp[i\hat{\boldsymbol{x}}\cdot\boldsymbol{\tau}F(r)], \qquad r = |\vec{x}|, \quad (3.10)$$

where $F(r)$ is the dimensionless function parametrizing the skyrmion profile. This is called the hedgehog ansatz in which the pion fields orient to a radial direction both in the position space and the isospin space. For the soliton energy to be finite as $r \to \infty$ and the ansatz to be regular at $r = 0$ we should impose the conditions as follows

$$F(r=\infty) = 0, \;\; F(r=0) = n\pi. \quad (3.11)$$

In terms of the chiral field U, these conditions read

$$U(r=0) = -1, \quad U(r=\infty) = 1. \quad (3.12)$$

Substituting the hedgehog ansatz into the winding number (the baryon number) Eq.(3.8), one can find the baryon number which the stable soliton has, to get

$$\begin{aligned} B &= \int d^3x j^0_W \\ &= -\left[\frac{1}{\pi}\left(F - \frac{1}{2}\sin 2F\right)\right]^{F(\infty)=0}_{F(0)=n\pi} \\ &= n. \end{aligned} \quad (3.13)$$

To descrive a single-baryon, we should set $n = 1$. Furthermore, the energy of a static soliton, called Skyrme energy $E_{\rm Skyr}$, is given by

$$E_{\rm Skyr} = -\int d^3x \mathcal{L}_{\rm Skyr}. \tag{3.14}$$

Substituting the hedgehog ansatz into the Skyrme energy, we have

$$E_{\rm Skyr} = 4\pi \int dr r^2 \left[\frac{f_\pi^2}{2} \left(2\frac{\sin^2 F}{r^2} + F'^2 \right) + \frac{\sin^2 F}{2g^2 r^2} \left(\frac{\sin^2 F}{r^2} + 2F'^2 \right) \right] \tag{3.15}$$

where the prime symbol attaching on F denotes the derivative with respect to r. From the Skyrme energy Eq.(3.15), the variational equation in terms of the Skyrme profile function F is obtained as

$$\left(r^2 + \frac{2}{g^2 f_\pi^2 \sin^2 F} F'' \right) + 2rF' + \frac{1}{g^2 f_\pi^2} \sin 2F F'^2 - \sin 2F - \frac{\sin^2 F \sin 2F}{g^2 f_\pi^2 r^2} = 0. \tag{3.16}$$

This equation can be solved in a numerical calculation, and then the Skyrme energy is evaluated as a function of the ratio of (f_π/g) with the exact numerical number (including an uncertainty due to a numerical systematics under which one works on)

$$E_{\rm Skyr} = 74.58... \times \left(\frac{f_\pi}{g} \right). \tag{3.17}$$

In addition, we can estimate the charge radius of the topologically stable soliton,

$$\begin{aligned} r_0 &= \left[\int d^3x r^2 j_W^0 \right]^{1/2} \\ &= \left[-\frac{2}{\pi} \int dr r^2 F' \sin^2 F \right]^{1/2}. \end{aligned} \tag{3.18}$$

Using the numerical solution of the profile function F, we also evaluate the charge radius of the topologically stable soliton as

$$r = 0.96... \times \left(\frac{1}{g f_\pi} \right). \tag{3.19}$$

Eq.(3.19) indicates that the skyrmion is the finite size object. However, this skyrmion is still a classical object, which means that the classical skyrmion does not have any quantum numbers such as the spin and the isospin. By quantizing the skyrmion, it is endowed with spin and isospin quantum numbers. Although we will not discuss the quantization of the skyrmion in

detail, a few remarks related to it will be made below.

Using $f_\pi = 92.4\,\mathrm{MeV}$ and $g = 5.93\,\mathrm{MeV}$ [42], the numerical result on the charge radius in Eq.(3.19) is obtained as $r \simeq 0.345\,\mathrm{fm}$, which is about 39% smaller than the experimental data of the nucleon, $r \simeq 0.877 \pm 0.005\,\mathrm{fm}$ [43] implying somewhat deviation from the experimental data, as have been suspected. However,we have a large N_c correction: the N_c counting can be assigned to the parameters, $f_\pi \sim \mathcal{O}(\sqrt{N_c})$ and $g \sim \mathcal{O}(1/\sqrt{N_c})$. Actually, the charge radius is of $\mathcal{O}(N_c^0)$. For $N_c = 3$, the next-to-leading order corrections would be on the size of $\mathcal{O}(1/N_c) \sim \mathcal{O}(0.3)$. Thus, the inclusion of possible large N_c corrections might make the model consistent with the experiments. Similarly, other numerical results based on the skyrmion approach are deviated from their experimental counterparts by 30% or 40% , which could also be cured by possible $1/N_c$ corrections. Thus, though being somewhat off from the realistic observations, one should keep one's mind that the skyrme model is still powerful and predictive when qualitative arguments related to the chiral symmetry structure are made.

3.3 Skyrmion-skyrmion interaction

The Skyrme's idea can be applied to a baryonic matter where skyrmions should be strongly bound by the attractive force among skymions. In this section we show how baryons interact with baryons interact with each other in terms of the skyrmion approach.

To describe baryonic matter based on the skyrmion approach, first, we should grasp how skyrmions strongly interact each other. And then, through analyzing the binding energy between two skyrmions, we shall deduce essential conditions in order to make up the baryonic matter based on the skyrmion approach.

In the beginning, we consider two skyrmions located at x_1 and x_2,

$$U_c(\boldsymbol{x} - \boldsymbol{x}_1), \;\; U_c(\boldsymbol{x} - \boldsymbol{x}_2), \tag{3.20}$$

which are placed far apart from each other. Since two skyrmions interact with each other, we rotate one skyrmion in isospin space, and then parametrize the topological configuration $U_{cc}(\boldsymbol{x}, \boldsymbol{x}_1, \boldsymbol{x}_2)$:

$$U_{cc}(\boldsymbol{x}, \boldsymbol{x}_1, \boldsymbol{x}_2) = U_c(\boldsymbol{x} - \boldsymbol{x}_1) C(\boldsymbol{\alpha}) U_c(\boldsymbol{x} - \boldsymbol{x}_2) C^\dagger(\boldsymbol{\alpha}), \tag{3.21}$$

where $C(\boldsymbol{\alpha}) = \exp(i\boldsymbol{\tau}\cdot\boldsymbol{\alpha}/2)$ represents the rotation matrix in the isopin space and α^a is the rotation parameter. The interaction between two skyrmions is controlled by the parameter α^a. For convenience, we introduce parameters a_0 and $a_{i=1,2,3}$, in such a way that the rotation matrix $C(\boldsymbol{\alpha})$ is parametrized as

$$C = a_0 + i\boldsymbol{a}\cdot\boldsymbol{\tau}. \tag{3.22}$$

By using Eqs.(3.20) and (3.21), the binding energy of two skymions is given as

$$V(\boldsymbol{x}_1, \boldsymbol{x}_2) = \int d^3x \left[\frac{1}{4} f_\pi^2 \mathrm{tr}[L_i(1,2)L_i(1,2)] + \frac{1}{32e^2}\mathrm{tr}\left[[L_i(1,2), L_j(1,2)]^2\right]\right] - E_1 - E_2, \tag{3.23}$$

where the first term, $V(\boldsymbol{x}_1, \boldsymbol{x}_2)+E_1+E_2$, represents the whole energy of two skyrmions, $E_{1,2}$ denote the energies of the isolated two skyrmions specified by $U_c(\boldsymbol{x} - \boldsymbol{x}_{1,2})$ and $L_\mu(1,2)$ is

$$L_\mu(1,2) = U_{cc}^\dagger(\boldsymbol{x}, \boldsymbol{x}_1, \boldsymbol{x}_2)\partial_\mu U_{cc}(\boldsymbol{x}, \boldsymbol{x}_1, \boldsymbol{x}_2). \tag{3.24}$$

For extremely separated skyrmions one can find the following binding energy,

$$V\left(r = |\boldsymbol{x}_1 - \boldsymbol{x}_2|\right) \sim A\frac{3(\boldsymbol{r}\cdot\boldsymbol{a})^2 - r^2\boldsymbol{a}^2}{r^5}, \tag{3.25}$$

with $r = |\vec{x}_1 - \vec{x}_2|$ and A being a constant. We can see in here that the conditions for the most attractive potential between two skyrmions are

$$\boldsymbol{r}\cdot\boldsymbol{a} = 0, \quad \boldsymbol{a}\cdot\boldsymbol{a} = 1. \tag{3.26}$$

Recalling the rotation matrix, $C = \exp(i\boldsymbol{\alpha}\cdot\boldsymbol{\tau}/2)$, these condition can be rewritten as

$$\begin{aligned} \boldsymbol{r}\cdot\boldsymbol{a} &= \frac{\boldsymbol{r}\cdot\boldsymbol{\alpha}}{|\boldsymbol{\alpha}|}\sin\frac{|\boldsymbol{\alpha}|}{2} = 0, \\ \boldsymbol{a}^2 &= \sin^2\frac{|\boldsymbol{\alpha}|}{2} = 1. \end{aligned} \tag{3.27}$$

In short, to obtain the most attractive potential for two skyrmions we should rotate one skyrmion in the isospin space by angle π around the axis perpendicular to the direction from one skyrmion to the other. When constructing the baryonic matter based on the skyrmion approach, we need to take account of this prescription.

3.4 Skyrmion crystal

Nuclear matter properties based on skyrmion approach have been investigated by Klebanov[32]. He proposed that the nuclear matter is formed out of skyrmions. This topological object identified as a baryonic matter is called skyrmion crystal in which the baryonic matter is described by putting skyrmions on lattice vertices of a crystal. In this section we briefly introduce the skyrmion crystal approach. And then, we shall show some phenomenological observables in the skyrmion crystal.

As premises for the introduction of skyrmion crystal approach, many-skyrmions are put on the crystal lattice vertices, where the centered-cubic crystal is conventionally chosen, and the size of the unit cell for a single crystal is $2L$. Looking at the two skyrmions located at (x, y, z) and $(x, y, z+2L)$, to produce the strongest attractive force for the nearest skyrmions, we should rotate the chiral field, $U(x, y, z + 2L)$, in a manner comparable to Eq.(3.27),

$$e^{-i\pi\tau_x/2}U(x, y, z + 2L)e^{i\pi\tau_x/2} = \tau_x U(x, y, z + 2L)\tau_x. \tag{3.28}$$

Since the cubic-crystal has the translation symmetry along the z-axis under $(x, y, z) \to (x, y, z + 2L)$, we have the periodic boundary condition for the chiral field,

$$U(x, y, z) = \tau_x U(x, y, z + 2L)\tau_x. \tag{3.29}$$

Similarly, the translational invariance for x- and y-axes gives us the boundary condition,

$$U(x, y, z) = \tau_y U(x + 2L, y, z)\tau_y = \tau_z U(x, y + 2L, z)\tau_z. \tag{3.30}$$

These conditions assure that the nearest skyrmions strongly interact with each other, so that the skyrmions take the crystal form.

3.4.1 Faced-centered cubic crystal

In this subsection, we focus on the faced-centered cubic (FCC) crystal for baryonic matter. The single-FCC crystal has the volum size $(2L)^3$ and contains 4-particles (4-baryons). In addition, the FCC crystal structure has the following discrete symmetries,

- Reflection symmetry: in position space $(x, y, z) \leftrightarrow (-x, y, z)$,
- Three fold symmetry:in position space $(x, y, z) \leftrightarrow (z, x, y)$,
- Four fold symmetry:in position space $(x, y, z) \leftrightarrow (y, -x, z)$,
- Translation symmetry: in position space $(x, y, z) \leftrightarrow (x + L, y + L, z)$.

(3.31)

To construct the FCC crystal from skyrmions, these symmetries should be reflected in isospin space. When mapping the three-dimensional space onto the isospin space for the chiral field, it is convenient to introduce pion fields $(\phi_0, \phi_{a=1,2,3})$ to expand the chiral field U as

$$U = \phi_0 + i\tau_a\phi_a, \tag{3.32}$$

which has the unitary relation,

$$(\phi_0)^2 + (\phi_a)^2 = 1. \tag{3.33}$$

We consider the static-skyrmion crystal, i.e. $\phi_\alpha(t,x,y,z) \equiv \phi_\alpha(x,y,z)$, Reflecting the intrinsic crystal symmetry on the chiral field U, the pion fields $(\phi_0, \phi_{a=1,2,3})$ have the following symmetries,

- Reflection symmetry:
  in position space $(x,y,z) \leftrightarrow (-x,y,z)$,
  in isospin space $(\phi_0,\phi_1,\phi_2,\phi_3) \leftrightarrow (\phi_0,-\phi_1,\phi_2,\phi_3)$,
- Three fold symmetry:
  in position space$(x,y,z) \leftrightarrow (z,x,y)$,
  in isospin space $(\phi_0,\phi_1,\phi_2,\phi_3) \leftrightarrow (\phi_0,\phi_3,\phi_1,\phi_2)$,
- Four fold symmetry:
  in position space $(x,y,z) \leftrightarrow (y,-x,z)$,
  in isospin space $(\phi_0,\phi_1,\phi_2,\phi_3) \leftrightarrow (\phi_0,\phi_2,-\phi_1,\phi_3)$,
- Translation symmetry:
  in position space$(x,y,z) \leftrightarrow (x+L,y+L,z)$,
  in isospin space $(\phi_0,\phi_1,\phi_2,\phi_3) \leftrightarrow (\phi_0,-\phi_1,-\phi_2,\phi_3)$.

(3.34)

The translation symmetry is related to the maximally attractive force between two adjacent skyrmions in terms of the FCC crystal, as discussed in Sec.3.3:

$$\begin{aligned} & \text{Boundary condition for FCC crystal:} \\ & U(x,y,z) = \tau_z U(x+L,y+L,z)\tau_z \\ \leftrightarrow \quad & \phi_0(x+L,y+L,z) + i\tau_a\phi_a(x+L,y+L,z) \\ & = \phi_0(x,y,z) - i\tau_1\phi_1(x,y,z) - i\tau_2\phi_2(x,y,z) + i\tau_3\phi_3(x,y,z). \end{aligned} \tag{3.35}$$

By using the symmetry properties listed as above, we shall simulate the skyrmion crystal. In the numerical simulation, it is convenient to introduce the unnormalized fields $\bar{\phi}_\alpha$ $(\alpha = 0,1,2,3)$, which are related to the normalized fields ϕ_α related to the unnormalized one $\bar{\phi}_\alpha$ as follows

$$\phi_\alpha = \frac{\bar{\phi}_\alpha}{\sqrt{\sum_{\beta=0}^{3} \bar{\phi}_\beta \bar{\phi}_\beta}}. \tag{3.36}$$

The unnormalized field $\bar{\phi}_\alpha$ is necessarily expanded by Fourier series [33]:

$$\begin{aligned}
\bar{\phi}_0(x,y,z) &= \sum_{a,b,c} \bar{\beta}_{abc} \cos(a\pi x/L)\cos(b\pi y/L)\cos(c\pi z/L) \\
\bar{\phi}_1(x,y,z) &= \sum_{h,k,l} \bar{\alpha}^{(1)}_{hkl} \sin(h\pi x/L)\cos(k\pi y/L)\cos(l\pi z/L) \\
\bar{\phi}_2(x,y,z) &= \sum_{h,k,l} \bar{\alpha}^{(2)}_{hkl} \cos(l\pi x/L)\sin(h\pi y/L)\cos(k\pi z/L) \\
\bar{\phi}_3(x,y,z) &= \sum_{h,k,l} \bar{\alpha}^{(3)}_{hkl} \cos(k\pi x/L)\cos(l\pi y/L)\sin(h\pi z/L), \qquad (3.37)
\end{aligned}$$

where $\bar{\beta}_{abc}$ and $\bar{\alpha}^{(1,2,3)}_{hkl}$ are the Fourir coefficients. Due to the symmetries of the FCC crystal in Eq.(3.34), the Fourier coefficients $\bar{\beta}_{abc}, \bar{\alpha}^{(1,2,3)}_{hkl}$ are constrained as follows[33] :

$$\begin{aligned}
\text{by three fold symmetry} &: \bar{\beta}_{abc} = \bar{\beta}_{bca} = \bar{\beta}_{cab}, \quad \bar{\alpha}^{(1)}_{hkl} = \bar{\alpha}^{(2)}_{hkl} = \bar{\alpha}^{(3)}_{hkl}; \\
\text{by four fold symmetry} &: \bar{\beta}_{abc} = \bar{\beta}_{acb} = \bar{\beta}_{cba} = \bar{\beta}_{bac}; \\
\text{by four fold symmetry} &: \bar{\alpha}_{hkl} = \bar{\alpha}_{hlk}; \\
\text{by translation symmetry} &: \text{a, b, c are all even numbers or odd numbers} \\
&\quad \text{and if h is even, then k, l are restricted to odd} \\
&\quad \text{numbers, otherwise even numbers.}
\end{aligned} \qquad (3.38)$$

In the isolated-skyrmion approach, we have imposed boundary conditions for the single-skyrmion to be stable and located at the position space where $(x, y, z) = (0, 0, 0)$, as discussed in Eq.(3.12). As for the skyrmion crystal approach, we should modify stability conditions for skyrmions. On the basis of stability conditions for isolated-skyrmion approach, the following conditions are placed

$$U(0,0,0) = -1, \quad U(L,0,0) = 1. \qquad (3.39)$$

These conditions imply that a single-skyrmion contained in FCC crystal is fixed at $(x, y, z) = (0, 0, 0)$. In addition, the Fourier coefficients $\bar{\beta}_{abc}$ is restricted by the stability condition. Inserting Eq.(3.37) into $U(0, 0, 0)$ and $U(L, 0, 0)$, we have

$$\begin{aligned}
U(0,0,0) &= \frac{\sum_{a,b,c} \bar{\beta}_{abc}}{\left|\sum_{a',b',c'} \bar{\beta}_{a'b'c'}\right|}, \\
U(L,0,0) &= \frac{\sum_{a,b,c} \bar{\beta}_{abc}(-1)^a}{\left|\sum_{a',b',c'} \bar{\beta}_{a'b'c'}(-1)^{a'}\right|}. \qquad (3.40)
\end{aligned}$$

To satisfy the boundary condition Eq.(3.39), the condition for the $\bar{\beta}_{abc}$ is imposed as

$$\sum_{a,b,c=\text{even}} \bar{\beta}_{abc} = 0. \tag{3.41}$$

In short, the Fourier coefficients $\bar{\beta}_{abc}, \bar{\alpha}^{(1,2,3)}_{hkl}$ are restricted by Eqs.(3.38) and (3.41), so that stable skyrmions are formed on a crystal lattice.

Next, using $f_\pi = 92.4\,\text{MeV}$ and $g = 5.93$ [42], we shall show the numerical result on the baryon energy per baryon E/N_B, which we will call "per-baryon energy",

$$\frac{E}{N_B} = -\frac{1}{4}\int_{\text{cube}} d^3x \mathcal{L}_{\text{Skyr}}, \tag{3.42}$$

with N_B being the baryon number. The per-baryon energy is evaluated as a function of the Fourier coefficients $\bar{\beta}_{abc}, \bar{\alpha}^{(i)}_{hkl}$, which are used as variational parameters in the numerical calculation. Those Fourier coefficients depending on the crystal size L are determined by minimizing the per-baryon energy thorough a numerical calculation, so that the per-baryon energy is obtained. And also, the numerical value of the Skyrme energy is saturated by only a few mode in the Fourier expansion. Therefore the higher modes are numerically negligible, and then in the numerical calculation we truncate the mode for the Fourier expansion until the per-baryon energy is saturated.

In Fig. 4.1 we show the per-baryon energy E/N_B as a function of the crystal size L. In low density region (corresponding in a large lattice size L), the value of the per-baryon energy should substantially be in accordance with the result from the isolated-skyrmion energy in Eq.(3.17). Actually, at $L = 2.0\,\text{fm}$, the per-baryon energy is $\simeq 1116\,\text{MeV}$ which is in a good agreement with the result on the isolated-skyrmion energy in Eq.(3.17), $E_{\text{Skyr}} = 74.58... \times (f_\pi/g) \simeq 1162\,\text{MeV}$. This implies that in an extremely low density region the binding energy obtained from skyrmion-skyrmion interaction in Eq.(3.25) is expected to be negligible. Conversely, in a high density region, the attractive force for skymions is relevant to the baryon energy. At $L = 0.85\,\text{fm}$, the per-baryon energy reaches the lowest value, $957\,\text{MeV}$. In other words, skyrmions are strongly bounded at $L = 0.85\,\text{fm}$.

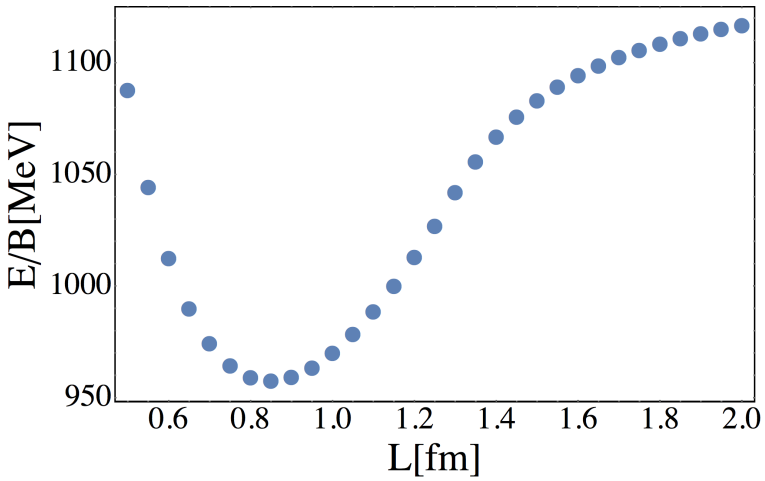

Figure 3.1: The matter dependence (the crystal size dependence) of the per-baryon energy.

3.4.2 Topological transition in baryonic matter

The skyrmion crystal approach predicts a characteristic phenomena which is called "topological phase transition". At some critical lattice size, this phase transition occurs in the skyrmion crystal. As a result, the FCC crystal structure changes to be of a completely different form. Below we remark the details on this transition phenomenon. .

When the baryon matter density estimated as $\rho = 4/(2L)^3$ increases, the FCC skyrmion crystal undergoes a phase transition in terms of the crystal-structure deformation. As was discussed in [33], in a low density region the skyrmion-crystal structure takes the FCC form, while in a high density region the skyrmion-crystal structure changes to be of the cubic-centered (CC) form. This structure change is triggered by the vanishing space-averaged value of ϕ_0,

$$\langle \phi_0 \rangle = \frac{1}{(2L)^3} \int_{-L}^{L} d^3x \phi_0, \tag{3.43}$$

hence the $\langle \phi_0 \rangle$ acts as if it were an order parameter and this phenomena can be phrased as a phase transition (topological phase transition). In terms of the phase transition, the low density region with the skyrmion crystal realized as the FCC form is called " skyrmion phase", while the high density region where the CC structure is manifest is called "half-skyrmion phase" (characterized by the transition density $\rho_{1/2}$), as dubbed in [33]. Note that the winding number, which is defined in a crystal lattice with size $2L$, is conserved, even after the structure/topology transition. When focusing on a single localized-topological object (single-skyrmion) in the skyrmion crystal,

it appears that a single-skyrmion has the winding number, "1". After the topological transition, it seems that the winding number of a single-skyrmion is changed to be "1/2", because the number of CC crystal is 4×8 in a crystal lattice with size 2L. In this sense, this transition is called "topology transition" in terms of a single localized-topological object in the crystal matter.

The presence of the half-skyrmion is robustly predicted from the viewpoint of the maximal discrete symmetry [50]. As we encounter the centered-cubic (CC) crystal, only the constraints on the Fourier coefficients from the translation symmetry as above is changed as

$$\begin{aligned} &\text{by translation symmetry : a, b, c are all odd numbers, and h is odd,} \\ &\qquad\qquad\qquad\qquad \text{then k, l are restricted even numbers.} \end{aligned} \tag{3.44}$$

This restriction for the chiral field indicates that after the the topological transition the skyrmion crystal has the following symmetry,

$$\begin{aligned} &- \text{ Translation symmetry:} \\ &\quad \text{in position space} (x, y, z) \ \leftrightarrow (x + L, y, z), \\ &\quad \text{in isospin space } \ (\phi_0, \phi_1, \phi_2, \phi_3) \leftrightarrow (-\phi_0, -\phi_1, \phi_2, \phi_3). \end{aligned} \tag{3.45}$$

Following this symmetry (condition), the skyrmion crystal configuration takes the CC crystal structure form.

The order parameter for the topological phase transition, $\langle \phi_0 \rangle$, can be rephrased as the space averaged value of the chiral condensate. The pion field configurations can be linked to quark field bilinears like,

$$\begin{aligned} \phi_0 &\sim \bar{q} q, \\ \phi_a &\sim \bar{q} i \gamma_5 \tau_a q. \end{aligned} \tag{3.46}$$

In terms of the vanishing chiral condensate, the vanishing ϕ_0 might be thought of as a signal for the chiral symmetry restoration, hence one might naively expect that the topological phase transition between the skyrmion phase and the half-skyrmion phase can be a direct link to the chiral restoration. However, the Skyme model is based on the nonlinear sigma model, so that the chiral symmetry can not be completely restored in this framework. Though it provides us with some qualitative features regarding the chiral symmetry, in that sense the $\langle \phi_0 \rangle$ cannot be thought of as the order parameter for the chiral symmetry.

In Fig. 3.2, we plot the space averaged value of ϕ_0 as a function of the crystal size L. The critical point of the topological transition shows up at $L_c \simeq 1.3\,\text{fm}$, which corresponds to the critical density $n_{1/2} \simeq 1.3 n_0$ with $n_0 \simeq 0.17/\text{fm}^3$ denoting the normal nuclear matter density ($L \simeq 1.4$[fm]).

Above the critical point $L_c \simeq 1.3\,\mathrm{fm}$, the $\langle\phi_0\rangle$ becomes smaller as the matter density increases (crystal size L decreases). Below the critical point $L_c \simeq 1.3\,\mathrm{fm}$, the vanishing $\langle\phi_0\rangle$ implies that the crystal structure is changed from the FCC structure to the CC structure. Actually, we can see the topological transition through the baryon number density j_B^0 as written in Eqs.(3.5) and (3.7). Next we shall show the skyrmion crystal configuration numerically.

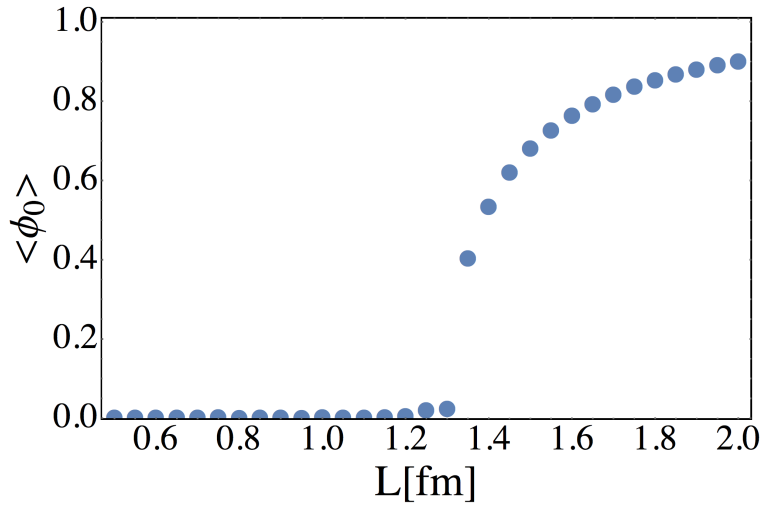

Figure 3.2: The matter dependence (crystal size dependence) of the order parameter for the topological phase transition, $\langle\phi_0\rangle$.

In the skyrmion crystal approach, the skyrmion crystal configuration can be visualized through the baryon-number density distribution $\rho_B = j_B^{\mu=0}$. In Fig. 3.3 we plot the baryon-number density distribution at $x-y$ plane, $\rho_B(x, y, 0)$. The left panel of Fig. 3.3 shows that in a low density region, where $L = 2.0\,\mathrm{fm}$, the skyrmion crystal forms the FCC structure. In contrast, one can easily find that in high density region, where $L = 1.0\,\mathrm{fm}$, the skyrmion crystal structure figures as the CC structure, as depicted in the right panel of the Fig. 3.3.

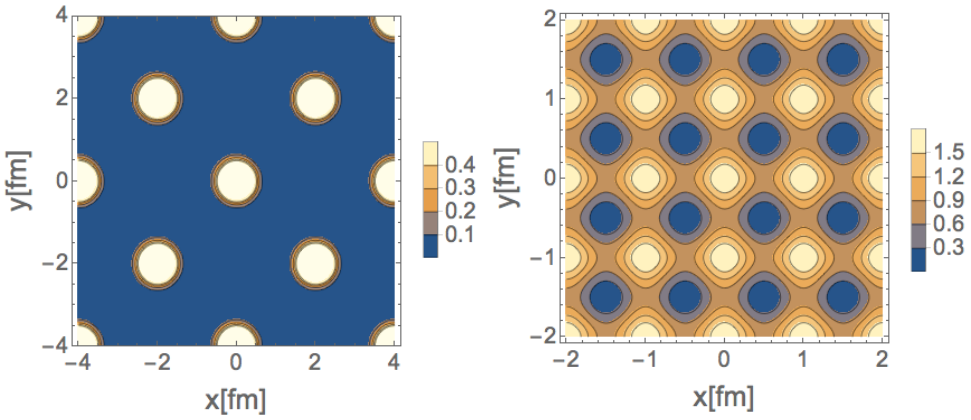

Figure 3.3: The baryon-number distribution, $\rho_B(x, y, 0)$, in the skyrmion phase where $L = 2.0\,\mathrm{fm}$ (left) and the half-skyrmion phase where $L = 1.0\,\mathrm{fm}$ (right).

3.4.3 Pion decay constant in skyrmion crystal

In the baryonic matter, the dynamical pions feel the matter effect, hence the pion decay constant gets the density dependence. In particular, the decreasing tendency of the pion decay constant in the baryonic matter is interpreted as the chiral restoration. In this section we discuss the density dependence on the pion decay constant in the skyrmion crystal.

To consider the pion decay constant in the skyrmion crystal, we shall introduce the fluctuating (dynamical) pion field as

$$\begin{aligned} U &= \breve{u}\bar{U}\breve{u}, \\ \breve{u} &= \exp\left(i\pi^a\tau^a/(2f_\pi)\right), \end{aligned} \tag{3.47}$$

where $\bar{U}$ denotes the static-skyrmion configuration and π^a describes the fluctuating pion field. Recall that the pion decay constant is defined in the matrix element of the axialvector current between the vacuum and the pion state as discussed in Eq.(2.28). In Skrme model, the axialvector current can be derived from the Lagrangian Eq.(4.2),

$$j^a_{A\mu} = \frac{F_\pi^2}{4}\mathrm{tr}\left[-i\left\{\frac{\tau^a}{2}, U\right\}\partial_\mu U^\dagger + i\left\{\frac{\tau^a}{2}, U^\dagger\right\}\partial_\mu U\right]. \tag{3.48}$$

Inserting the chiral field Eq.(3.47) into this current, we have

$$j^a_{A\mu=0} = -f_\pi\partial_0\pi^b\left[(\phi_0)^2\delta^{ab} + \phi^a\phi^b\right] + \mathcal{O}(\pi^2). \tag{3.49}$$

This current form shows that the axialvector current indicates the static-skyrmion configuration. Therefore, we can deduce that the pion decay

constant is modified by the static-skymion configuration. Actually, in the skyrmion crystal, the matrix element reads

$$\langle 0|j^{a=3}_{A\mu=0}|\pi^{b=3}(p)\rangle = if_\pi p_0(1-\langle\phi_0^2\rangle)e^{ip\cdot x}. \tag{3.50}$$

To incorporate the matter effect into the pion dynamics, the fluctuating pion field π should be canonically normalized as

$$\pi^* = \frac{1}{\sqrt{1-\frac{2}{3}(1-\langle\phi_0^2\rangle)}}\,\pi. \tag{3.51}$$

Then the matrix element is described as

$$\langle 0|j^{a=3}_{A\mu=0}|\pi^{*b=3}(p)\rangle = if^*_\pi p_0 e^{ip\cdot x}, \tag{3.52}$$

where f^*_π is the modified pion decay constant,

$$f^*_\pi \;=\; \sqrt{1-\frac{2}{3}(1-\langle\phi_0^2\rangle)}\,f_\pi. \tag{3.53}$$

To obtain Eq.(3.53), we have used the unitary relation $(\phi_0)^2+(\phi_a)^2=1$. And also, we have introduced the space averaged values of the static-skyrmion configuration,

$$\langle X\rangle = \frac{1}{(2L)^3}\int_{\rm cube} d^3x\, X, \tag{3.54}$$

where X is an arbitrary operator constructed from the static-skyrmion configuration and $\int_{\rm cube} d^3x = \int_{-L}^{L} dx \int_{-L}^{L} dy \int_{-L}^{L} dz$. The modified pion decay constant f^*_π in Eq.(3.53) indicates that the pion decay constant gets the density effect through the contribution of the static-skyrmion configuration.

In Fig. 3.4, we plot the pion decay constant normalized to the matter-free value, f^*_π/f_π, which is a function of the crystal size of L. As the matter density increases, the pion decay constant gets smaller up to the critical point $L_c \simeq 1.3\,\text{fm}$ corresponding to $n_{1/2} \simeq 1.3 n_0$. After the critical point, the pion decay constant is reflected by the vanishing $\langle\phi_0\rangle$, so that the value of f^*_π/f_π undergoes very little change. Even in a high density region, the pion decay constant remains the finite value, hence this result show that the chiral symmetry is partially restored (the chiral symmetry is not completely restored).

Now, we should comment on the chiral symmetry restoration based on the Skyrmoin crystal approach. Recall that in high density region the value of $\langle\phi_0\rangle$ vanishes, as depicted in Fig.3.2. Although the $\langle\phi_0\rangle$ can be linked with the space averaged value of chiral condensate as discussed previously in Eq.(3.46), the vanishing $\langle\phi_0\rangle$ does not signal the chiral symmetry restoration. From the viewpoint of the matter dependence on the pion decay constant, the decreasing behavior of the modified pion decay constant, f^*_π/f_π,

implies that the chiral symmetry is partially restored in the skyrmion crystal. However, the modified pion decay constant remains a finite value at a high density region, hence we can suspect that the chiral symmetry is still broken.

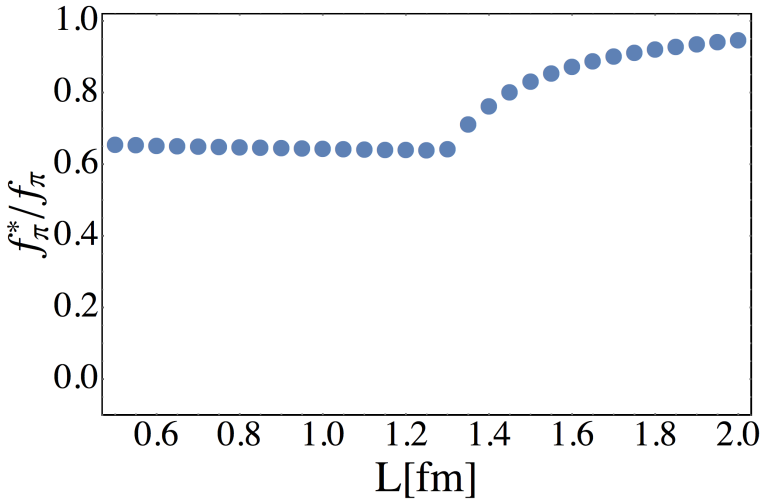

Figure 3.4: The pion decay constant in the skyrmion crystal normalized to the matter-free value, f_π^*/f_π.

In closing this chapter, we shall give a few comments on the phenomenological implications from the skyrmion crystal approach. At a low density region below the normal nuclear density, the prevalent picture of nuclear matter is the Fermi-liquid structure in which the nuclear matter is expected to be described as liquid drops or hadron gas. In contrast, at a high-density region nucleons are nearly compressed and then a nucleon should be fixed at a position. Therefore, the fixed nucleon can be treated as static objects with the large N_c limit, so that at a high density region the skyrmoin crystal could be a proper description, and will be more powerful to analyze such a highly dense-matter physics.

Chapter 4

Magnetic effect on skyrmion crystal

We explore the magnetic properties of a baryonic matter based on the skyrmion crystal model. By applying the magnetic field to the skyrmion crystal, it turns out that the skyrmion intrinsic properties and related ones (Skyrme energy, topological phase transition, pion decay constant and skyrmion configuration) are drastically changed. In addition, the inhomogeneity for the chiral condensate in the skyrmion crystal gets the magnetic dependence.

4.1 Skyrme model with a magnetic field

First, to analyze the magnetic effect on the skyrmion crystal, we consider to incorporate a magnetic field into the Skyrme model. By gauging the chiral symmetry in part, one can freely introduce the external magnetic field in the Skyrme model. Then, the derivative of the chiral field U is changed to be a covariantized version :

$$D_\mu U = \partial_\mu U - ieA_\mu[Q_E, U], \tag{4.1}$$

where e is the unit of electric charge and $Q_E = \frac{1}{6}\cdot 1_{2\times 2} + \frac{1}{2}\tau_3$ is the electric charge matrix for the $(u,d)^T$ $SU(2)$ doublet quark field with τ_3 being the third component of the Pauli matrix. In this study, we consider a constant magnetic field (B) along the z direction. The Skyrme Lagrangian including an external magnetic field is then given as

$$\mathcal{L}_{\text{Skyr}} = \frac{f_\pi^2}{4}\text{tr}[D_\mu U D^\mu U^\dagger] + \frac{1}{32g^2}\text{tr}\Big([U^\dagger D_\mu U, U^\dagger D_\nu U][U^\dagger D^\mu U, U^\dagger D^\nu U]\Big) \tag{4.2}$$

The presence of a magnetic field along the z-axis breaks the $O(3)$ symmetry down to the $O(2)$ symmetry. To respect the residual $O(2)$ symmetry

for the $x-y$ plane, we choose the symmetric gauge: [1]

$$A_\mu = -\frac{1}{2}By\delta_\mu{}^1 + \frac{1}{2}Bx\delta_\mu{}^2. \tag{4.3}$$

Hereafter we shall apply the FCC crystal conditions as written in Eqs.(3.37) and (3.38) to study the skyrmion crystal properties in a magnetic field.

4.1.1 How to implement a magnetic field in skyrmion crystal approach

Looking at the covariant derivative of the chiral field U written as

$$D_\mu U = \partial_\mu\phi_0 + iD_\mu\phi_1\tau_1 + iD_\mu\phi_2\tau_2 + i\partial_\mu\phi_3\tau_3, \tag{4.4}$$

where $D_\mu\phi_1 = \partial_\mu\phi_1 - eA_\mu\phi_2$ and $D_\mu\phi_2 = \partial_\mu\phi_2 + eA_\mu\phi_1$, we note that a covariant derivative operator such as $D_x\phi_1$ has to be discretized so as to hold the translational invariance in the x-y plane. As for $y\bar{\phi}_2(x,y,z)$, its Fourier transform is thus evaluated as follows:

$$\begin{aligned}
&y\bar{\phi}_2(x,y,z)\\
&= y\int_{-\infty}^{\infty}\frac{dp_x}{(2\pi)}\int_{-\infty}^{\infty}\frac{dp_y}{(2\pi)}\int_{-\infty}^{\infty}\frac{dp_z}{(2\pi)}\bar{\phi}_2(p_x,p_y,p_z)e^{i\vec{p}\cdot\vec{x}}\\
&= \int_0^{\infty}\frac{dp_x}{(2\pi)}\int_0^{\infty}\frac{dp_y}{(2\pi)}\int_0^{\infty}\frac{dp_z}{(2\pi)}\bar{\phi}_2(p_x,p_y,p_z)8i\cos(p_xx)\left(-\partial_{p_y}\cos(p_yy)\right)\cos(p_zz)\\
&\xrightarrow{\text{discretization}} -\sum_{h,k,l}\bar{\alpha}^{(2)}_{h,k,l}\cos(l\pi x/L)\frac{\cos\{(h+2)\pi y/L\}-\cos(h\pi y/L)}{2\pi/L}\cos(k\pi z/L)\\
&\equiv [y\bar{\phi}_2]_{\text{disc}}(x,y,z),
\end{aligned} \tag{4.5}$$

where we have used the reflection symmetry (see Eq.(3.31)) in the second equality. Now we make the translation for $[y\bar{\phi}_2]_{\text{disc}}(x,y,z)$ as (see Eq.(3.34))

$$[y\bar{\phi}_2]_{\text{disc}}(x,y,z) \xrightarrow{\text{translation:}(x,y,z)\to(x+L,y+L,z)} -[y\bar{\phi}_2]_{\text{disc}}(x,y,z). \tag{4.6}$$

[1] When we work on the skyrmion crystal having a magnetic field, it is necessary to choose the symmetric gauge to hold the $O(2)$ symmetry. We can see this kind of gauge-dependent issue also in the ladder approximation approaches, where by fixing the some suitable gauge choice QCD observables related to the chiral symmetry are computed and observed.

This is obviously of a covariant form. In this study we use $[y\bar{\phi}_2]_{\rm disc}$ instead of $y\bar{\phi}_2$. In a similar way one can get the following discretization forms:

$$\begin{aligned}
[x\bar{\phi}_1]_{\rm disc}(x,y,z) &= -\sum_{h,k,l}\bar{\alpha}_{h,k,l}\frac{\cos\{(h+2)\pi x/L\}-\cos(h\pi x/L)}{2\pi/L}\cos(k\pi y/L)\cos(l\pi z/L)\\
[y\bar{\phi}_1]_{\rm disc}(x,y,z) &= \sum_{h,k,l}\bar{\alpha}_{h,k,l}\sin(h\pi x/L)\frac{\sin\{(k+2)\pi y/L\}-\sin(k\pi y/L)}{2\pi/L}\cos(l\pi z/L)\\
[x\bar{\phi}_2]_{\rm disc}(x,y,z) &= \sum_{h,k,l}\bar{\alpha}_{h,k,l}\frac{\sin\{(l+2)\pi x/L\}-\sin(l\pi x/L)}{2\pi/L}\sin(h\pi y/L)\cos(k\pi z/L).
\end{aligned} \tag{4.7}$$

With the prescribed discretization method at hand, let us check whether the other symmetries in the FCC crystal are kept in the presence of a magnetic field. For instance, the covariant derivative of ϕ_1 is transformed as

$$[D_i\phi_1]_{\rm disc}(x,y,z) \xrightarrow{\text{reflection: } (x,y,z)\to(-x,y,z)} \begin{cases}(i=x) & [D_x\phi_1]_{\rm disc}(x,y,z)\\ (i=y) & -[D_y\phi_1]_{\rm disc}(x,y,z)\\ (i=z) & -[D_z\phi_1]_{\rm disc}(x,y,z)\end{cases}$$

$$[D_i\phi_1]_{\rm disc}(x,y,z) \xrightarrow{\text{translation:}(x,y,z)\to(x+L,y+L,z)} -[D_i\phi_1]_{\rm disc}(x,y,z)$$

$$[D_i\phi_1]_{\rm disc}(x,y,z) \xrightarrow{\text{two fold for z axis:}(x,y,z)\to(y,-x,z)} \begin{cases}(i=x) & (\partial_y\phi_2+eA_y\phi_1)_{\rm disc}(x,y,z)\\ (i=y) & -(\partial_x\phi_2+eA_x\phi_1)_{\rm disc}(x,y,z)\\ (i=z) & [D_z\phi_2]_{\rm disc}(x,y,z)\end{cases}$$

$$[D_i\phi_1]_{\rm disc}(x,y,z) \xrightarrow{\text{two fold for x axis:}(x,y,z)\to(x,z,-y)} \begin{cases}(i=x) & (\partial_x\phi_1-eA_x\phi_3)_{\rm disc}(x,y,z)\\ (i=y) & (\partial_z\phi_1-eA_z\phi_3)_{\rm disc}(x,y,z)\\ (i=z) & -(\partial_y\phi_1-eA_y\phi_3)_{\rm disc}(x,y,z)\end{cases}$$

$$[D_i\phi_1]_{\rm disc}(x,y,z) \xrightarrow{\text{three fold:}(x,y,z)\to(z,x,y)} \begin{cases}(i=x) & (\partial_z\phi_3-eA_z\phi_1)_{\rm disc}(x,y,z)\\ (i=y) & (\partial_x\phi_3-eA_x\phi_1)_{\rm disc}(x,y,z)\\ (i=z) & (\partial_y\phi_3-eA_y\phi_1)_{\rm disc}(x,y,z)\end{cases}. \tag{4.8}$$

One can see easily that a magnetic field along the z axis explicitly breaks the two fold symmetry for the $x(y)$ axis and the three fold symmetry. Thus,

through this discretization way, the explicit symmetry breaking, by which the $O(3)$ symmetry is broken to the $O(2)$ symmetry by a magnetic field, is reflected in the discrete symmetries of the FCC crystal.

4.1.2 A baryon number density induced by a magnetic field

In the skyrmion approach without a magnetic field, the baryon current is equivalent to the topological current, as discussed in Eq.(3.7). In contrast, turning on a magnetic field, the baryon current is not the same as the topological current, because the presence of a magnetic field modifies the baryon current form. In this section, we show the correction part for the baryon current, induced by a magnetic field

Even in a constant magnetic field (eB), the baryon current can be extracted in a way similar to Eq.(3.7):

$$j_B^\mu(eB) = \left.\frac{\partial \Gamma_{WZW}}{\partial \mathcal{V}_{B\mu}}\right|_{\mathcal{V}_{B\mu}\to 0}. \tag{4.9}$$

One can find the baryon current in the presence of a magnetic field [44],

$$j_B^\mu = j_W^\mu + \mathcal{J}_{eB}^\mu, \tag{4.10}$$

where

$$\begin{aligned} j_W^\mu &= \frac{1}{24\pi^2}\epsilon^{\mu\nu\rho\sigma}\mathrm{tr}\Big[(\partial_\nu U\cdot U^\dagger)(\partial_\rho U\cdot U^\dagger)(\partial_\sigma U\cdot U^\dagger)\Big], \\ \mathcal{J}_{eB}^\mu &= \frac{1}{16\pi^2}\epsilon^{\mu\nu\rho\sigma}\mathrm{tr}\Big[ie(\partial_\nu A_\rho)Q_E(\partial_\sigma U\cdot U^\dagger + U^\dagger\partial_\sigma U) \\ &\quad + ieA_\nu Q_E(\partial_\rho U\partial_\sigma U^\dagger - \partial_\rho U^\dagger\partial_\sigma U)\Big], \end{aligned} \tag{4.11}$$

in which j_W^μ corresponds to the topological current and $\mathcal{J}_{eB}^\mu$ denotes the induced baryon current by a magnetic field. By taking the symmetric gauge in Eq.(4.3), the time component of the induced baryon current is evaluated as follows

$$\begin{aligned} \mathcal{J}_{eB}^0 &= \left[\frac{-eB}{4\pi^2}\big\{(\partial_z\phi_3)\phi_0 - (\partial_z\phi_0)\phi_3\big\}\right] \\ &\quad + \left[\frac{+eB}{8\pi^2}\big\{[y\partial_y\phi_3]_{\mathrm{disc}}(\partial_z\phi_0) - [y\partial_y\phi_0]_{\mathrm{disc}}(\partial_z\phi_3)\big\}\right. \\ &\quad \left. + \frac{-eB}{8\pi^2}\big\{(\partial_z\phi_3)[x\partial_x\phi_0]_{\mathrm{disc}} - (\partial_z\phi_0)[x\partial_x\phi_3]_{\mathrm{disc}}\big\}\right]. \end{aligned} \tag{4.12}$$

In Eq.(4.12), we have used the discretized form with a derivative operator such as $[y\partial_y\phi_3]_{\rm disc}$ (the explicit expressions are supplied in Appendix E). Then, the modified total-baryon number density, $\rho_B(x,y,z)$, is expressed as

$$\begin{aligned}\rho_B(x,y,z) &= j^0_W(x,y,z) + \mathcal{J}^0_{eB}(x,y,z) \\ &\equiv \rho_W(x,y,z) + \tilde{\rho}_{eB}(x,y,z),\end{aligned} \tag{4.13}$$

where $\rho_W(z,y,z)$ represents the winding number density and $\tilde{\rho}_{eB}(x,y,z)$ denotes the induced-baryon number density driven by the presence of a magnetic field. By performing the spacial integration for the baryon number density, ρ_B, one can obtain the baryon number within a single-FCC crystal:

$$N_B = \int_{\rm cube} d^3x\rho_B. \tag{4.14}$$

A single-FCC crystal has the volume size $(2L)^3$ and contains 4 skyrmions. Even though a magnetic field is present, the baryon number in a single FCC crystal is conserved because $\int_{\rm cube}\tilde{\rho}_{eB} = 0$ [2], namely,

$$N_B = \int_{\rm cube} d^3x\rho_B = \int_{\rm cube} d^3x\rho_W = 4. \tag{4.15}$$

4.2 Analysis of magnetic dependences in skyrmion crystal

In this section we numerically study the magnetic dependence of the per-baryon energy, and the order parameter of the topological phase transition, together with its related phenomena such as the inhomogeneity of the chiral condensate, as well as the pion decay constant in the skyrmion crystal. Also the deformation of the skyrmion configuration will be discussed by examining the magnetic dependence on the baryon number density, ρ_B.

4.2.1 Per-baryon energy E/N_B in a magnetic field

After fixing the strength of a magnetic field, we evaluate the per-baryon energy as a function of the Fourier coefficients $\bar{\beta}_{abc}$, $\bar{\alpha}^{(i)}_{hkl}$. When minimizing

[2] Using Eqs.(3.37) and (3.38), one can derive the following equations,

$$\begin{aligned}\int_{\rm cube} d^3x\,(\partial_z\phi_3)\phi_0 = \int_{\rm cube} d^3x\,\phi_3\partial_z\phi_0 &= 0 \\ \int_{\rm cube} d^3x\,[y(\partial_y\phi_3)]_{\rm disc}\,(\partial_z\phi_0) = \int_{\rm cube} d^3x\,[y(\partial_y\phi_0)]_{\rm disc}\,(\partial_z\phi_3) &= 0 \\ \int_{\rm cube} d^3x\,[x(\partial_x\phi_3)]_{\rm disc}\,(\partial_z\phi_0) = \int_{\rm cube} d^3x\,[x(\partial_x\phi_0)]_{\rm disc}\,(\partial_z\phi_3) &= 0.\end{aligned}$$

To derive above equations, we have used the same Fourier expansion form for ϕ_α as that for $\bar{\phi}_\alpha$, as in Eq.(3.37). Thus one can find $\int_{\rm cube}\mathcal{J}^0_B(eB) = 0$, hence the baryon number in the FCC crystal keeps being 4 in a magnetic field.

the per-baryon energy through the numerical calculation, those Fourier coefficients depend on the crystal size L and a magnetic strength eB. In this study, we take the values of the parameters as $f_\pi = 92.4$[MeV], $g = 5.93$ [42].

In Fig.4.1 we plot the per-baryon energy as a function of the crystal size with the strength of the magnetic field varied[3]. Note first that Fig. 4.1 precisely reproduces the result in [33] on the crystal-size dependece of the per-baryon energy without the magnetic field ($eB = 0$), as it should. When the magnetic field is turned on to be increasing, the per-baryon energy increases for any crystal size L. In particular, for the low density region (large crystal size L), we should compare this tendency with that obtained in [44] based on the single-skyrmion approach, not on the crystal (not in a medium). The energy of the isolated-skyrmion obtained in [44] has a minimum energy with respect to the strength of a magnetic field, eB, because a destructive interference arises between terms of $\mathcal{O}(eB)$ and $\mathcal{O}\big((eB)^2\big)$ in the per-baryon energy functional, E/N_B. In contrast it is not the case for our per-baryon energy: $\mathcal{O}(eB)$ terms drop when the per-baryon energy functional is integrated over the volume of the crystal. For example, the Skyrme model with a magnetic field has $\mathcal{O}(eB)$ terms like

$$eA_i\phi_2\partial_i\phi_1 = eA_x\phi_2\partial_x\phi_1 + eA_y\phi_2\partial_y\phi_1. \tag{4.16}$$

By using Eqs.(3.37) and (3.38), the space averaged value of $\mathcal{O}(eB)$ goes to zero:

$$\frac{1}{(2L)^3}\int_{\rm cube} d^3x eA_x\phi_2\partial_x\phi_1 \;=\; -\frac{eB}{2}\frac{1}{(2L)^3}\int_{\rm cube} d^3x\,[y\phi_2]_{\rm disc}\partial_x\phi_1 = 0. \tag{4.17}$$

Likewise, the integration for $eA_y\phi_2\partial_y\phi_1$ also vanishes. Thus, only $\mathcal{O}\big((eB)^2\big)$ terms remain in the per-baryon energy. This magnetic dependence of the per-bayron energy is reflected in Fig 4.1.

In a low density region such as at $L = 2.0$[fm], the per-baryon energy is quite enhanced by the external magnetic field. Conversely, in a high density region around $L = 0.5$[fm], the per-baryon energy undergoes very little change. To grasp this tendency the position space is rescaled by the crystal size: $x = x'/L$, to rewrite the covariant derivative $D_x\phi_1 = (\partial_{x'}\phi_1 + i\frac{eBL^2}{2}y'\phi_2)/L$ in the per-baryon energy functional. Thus, the magnetic dependence of the per-baryon energy becomes negligible, as the crystal size gets narrow, which is certainly reflected in Fig.4.1.

[3]Throughout the present analysis, we have cut the largest size of $\sqrt{eB}$ at 800[MeV] just because of some computational issue.

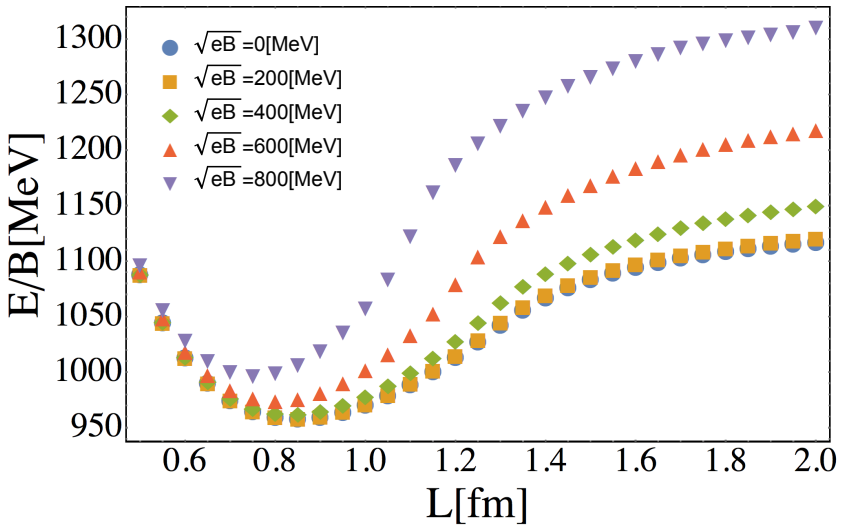

Figure 4.1: The per-baryon energy in a magnetic field as a function of the crystal size L.

4.2.2 Magnetic effect on topological phase transition and inhomogeneity of chiral condensate

In the present subsection, we first discuss the magnetic dependence of this topological phase transition. Furthermore, we also address to the inhomogeneity of the chiral condensate affected by a magnetic field. Fig. 4.2 shows the magnetic dependence on the order parameter for the topological transition, $\langle\phi_0\rangle$. As the magnetic field increases, the phase transition point is shifted to a high density region. For instance, the critical density is observed at $n_{1/2} \simeq 2.2n_0$ when the strength of a magnetic field is $\sqrt{eB} = 800$[MeV]. Meanwhile, the value of the order parameter becomes larger for any crystal size. This implies the magnetic catalysis for the topological phase transition. Furthermore, one can rephrase this enhancement for the $\langle\phi_0\rangle$ as the magnetic catalysis regarding the space averaged value of the chiral condensate, by recalling the relation between $\langle\phi_0\rangle$ and $\langle\bar{q}q\rangle$ as written in Eq.(3.46).

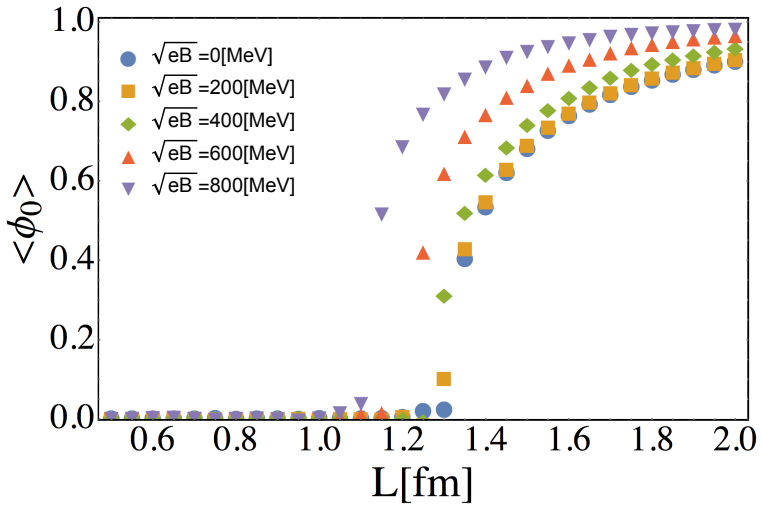

Figure 4.2: The order parameter for the topological, $\langle\phi_0\rangle$, in a magnetic field, as a function of the crystal size L.

Besides the topological phase transition of interest is also to notice that ϕ_0 and $\phi_{a=1,2,3}$ (see Eq.(3.46)) have the spatial distribution, hence the chiral condensate has the inhomogneous distribution. Actually, one can interpret this spatial distributions of the ϕ_0 and $\phi_{a=1,2,3}$ as a sort of inhomogeneous chiral condensate. See Figs. 4.3 and 4.4, which display the magnetic effect on the distributions of $\phi_0(x,y,z)$ and $\phi_1(x,y,z)$ in low density region where $L = 2.0$[fm] (corresponding to the skyrmion phase). The panels labeled by (a) in those figures show the presence of the inhomogeneities of ϕ_0 and ϕ_1 without the magnetic field ($eB = 0$), where the configurations of the inhomogeneous chiral condensate are read as a "pulse" form for the $\phi_0(\sim \bar{q}q)$ and a "wave" form for the $\phi_1(\sim \bar{q}i\gamma_5\tau^1 q)$. These results are in agreement with the analysis in [45]. Switching on the magnetic field (panels (b) and (c)), a remarkable phenomenon appears. As the strength of a magnetic field increases, the inhomogeneous distribution of ϕ_0 and ϕ_1 will be remarkably localized while keeping each underlying shape of the "pulse"- and "wave-" like form. Focusing on the $y = z = 0$ plane, the configurations of inhomogeneous chiral condensate capture this novel tendency, as depicted in Fig. 4.5. In different models (approaches) [46, 47, 48, 49], similar behavior, associated with the magnetic effect on the inhomogeneous chiral condensate, have been observed.

Next see Figs. 4.6 and 4.7, which draw the magnetic dependence on the distributions of $\phi_0(x,y,z)$ and $\phi_1(x,y,z)$ in a high density region where $L = 1.0$[fm] (corresponding to the half-skyrmion phase). In those figures the panels (a) tell us that the inhomogeneities of ϕ_0 and ϕ_1 without the magnetic field ($eB = 0$) are present. This is, again, in accord with the

analysis in [45]. With the magnetic field switched on (panels (b) and (c)), one can find that the ϕ_0 and ϕ_1 inhomogeneities still survive when eB gets larger. In contrast to the skyrmion phase, the inhomogeneities of ϕ_0 and ϕ_1 get hardly influenced by the strength of a magnetic field (see Fig. 4.8).

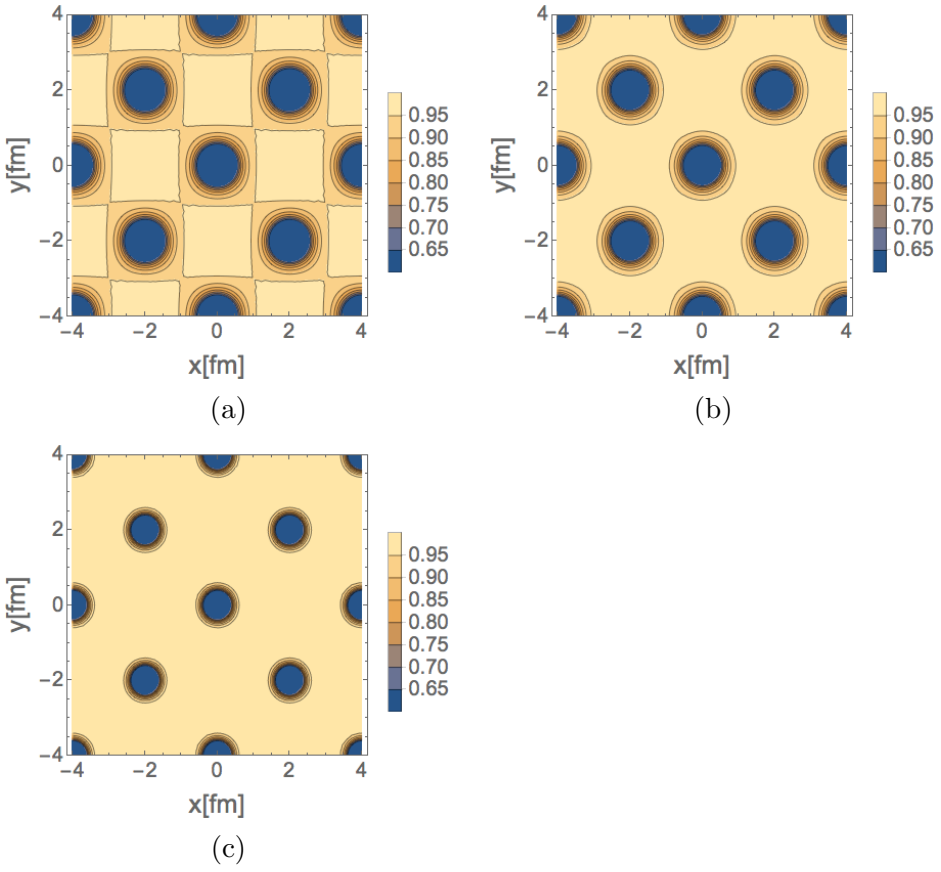

Figure 4.3: The distributions of $\phi_0(x, y, 0)$ at $L = 2.0$ fm (in the skyrmion phase). (a): $\sqrt{eB} = 0$. (b): $\sqrt{eB} = 400$ MeV. (c): $\sqrt{eB} = 800$ MeV.

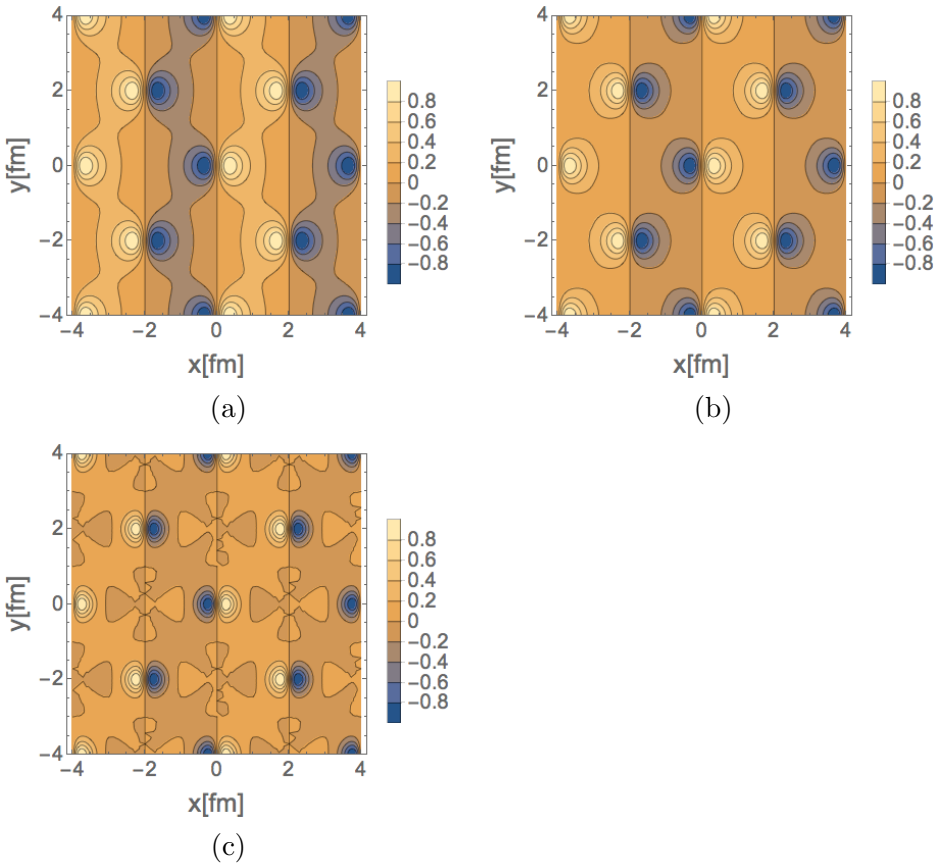

Figure 4.4: The distributions of $\phi_1(x, y, 0)$ at $L = 2.0$[fm] (in the skyrmion phase). (a): $\sqrt{eB} = 0$ MeV. (b): $\sqrt{eB} = 400$ MeV. (c): $\sqrt{eB} = 800$ MeV.

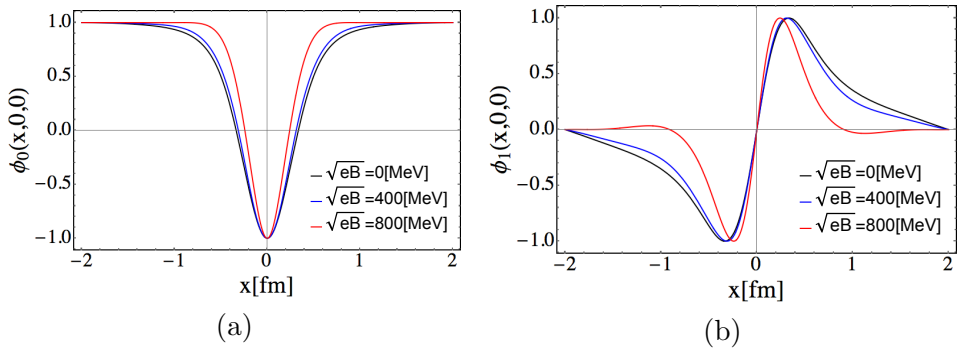

Figure 4.5: The distributions of $\phi_0(x, 0, 0)$ (panel (a)) and $\phi_1(x, 0, 0)$ (panel (b)) at $L = 2.0$[fm] (in the skyrmion phase) with $\sqrt{eB}$ varied.

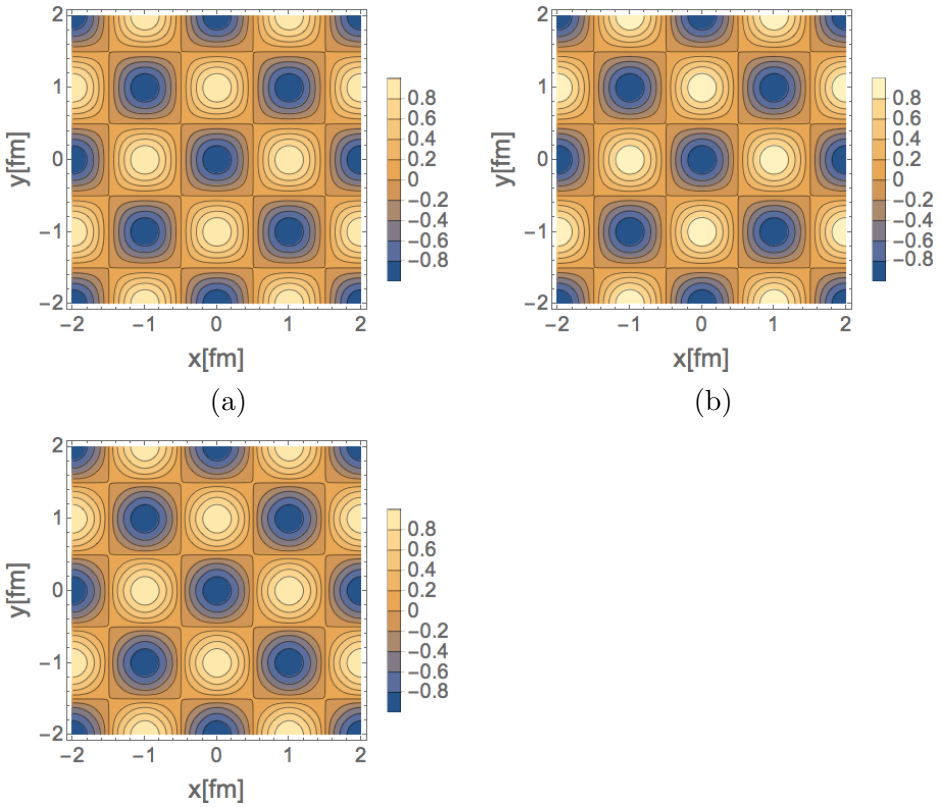

Figure 4.6: The distributions of $\phi_0(x, y, 0)$ at $L = 1.0$[fm] (in the half-skyrmion phase). (a): $\sqrt{eB} = 0$[MeV]. (b): $\sqrt{eB} = 400$[MeV]. (c): $\sqrt{eB} = 800$[MeV].

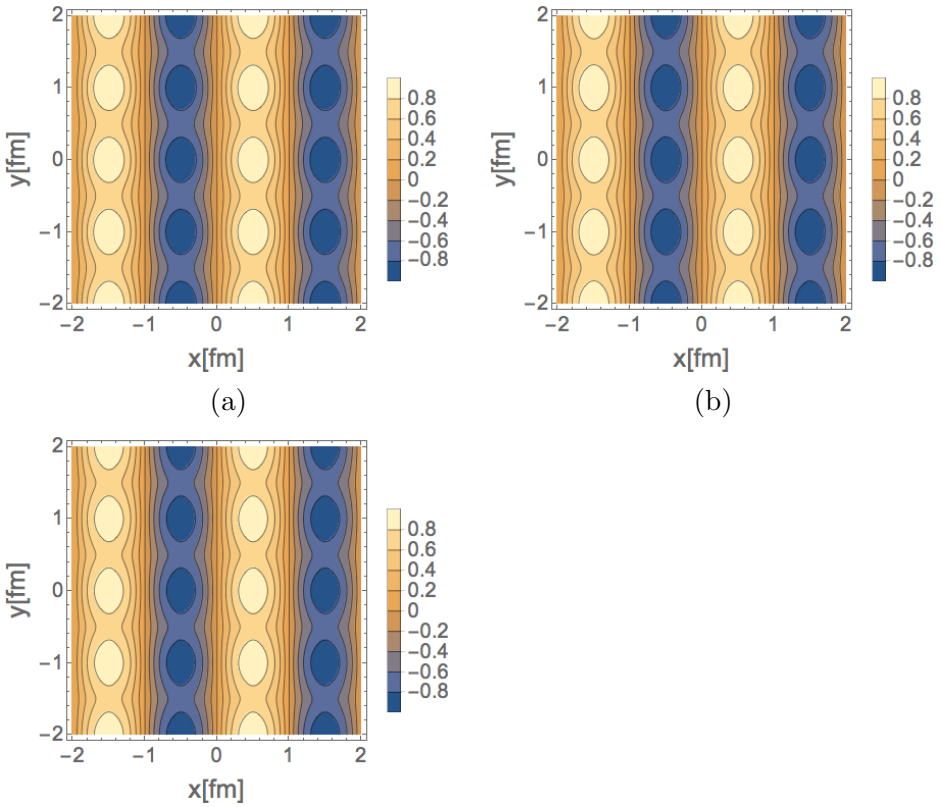

Figure 4.7: The distributions of $\phi_1(x, y, 0)$ at $L = 1.0$[fm] (in the half-skyrmion phase). (a): $\sqrt{eB} = 0$[MeV]. (b): $\sqrt{eB} = 400$[MeV]. (c): $\sqrt{eB} = 800$[MeV].

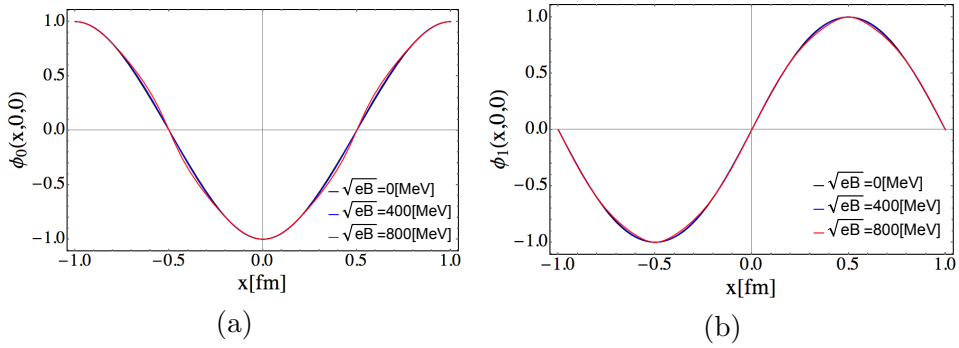

Figure 4.8: The distributions of $\phi_0(x, 0, 0)$ (panel (a)) and $\phi_1(x, 0, 0)$ (panel (b)) at $L = 1.0$[fm] (in the half-skyrmion phase) with $\sqrt{eB}$ varied.

4.2.3 Magnetic dependence on pion decay constant

As mentioned above, the magnetic behavior of $\langle\phi_0\rangle$ indicates that the vanishing $\langle\bar{q}q\rangle$ tends to shift to the high density region (see Fig. 4.2). In this subsection, we analyze the magnetic effect on the (partial) chiral symmetry restoration in terms of the pion decay constant.

Fig. 4.9, as a magnetic field increases, the critical point of the pion decay constant tends to get shifted to be in a higher density region. This tendency is the same as what the the $\langle\phi_0\rangle$ has Fig. 4.2, as it should be. In addition, one can find the enhancement for the value of the pion decay constant in increasing the strength of a magnetic field. Thus, the magnitude of the chiral symmetry breaking is enhanced by a magnetic field. This tendency implies that the magnetic field plays the role of catalyzer for the chiral symmetry breaking, as discussed in [51].

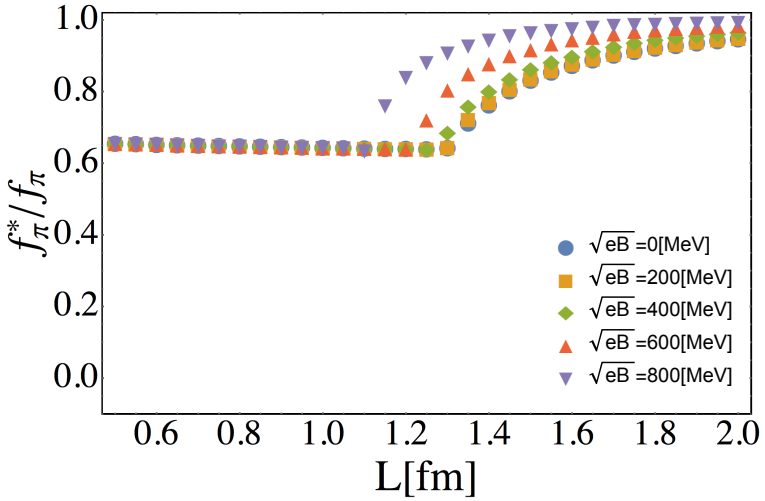

Figure 4.9: The pion decay constant in the skyrmion crystal normalized to the matter-free value, f_π^*/f_π, in a magnetic field plotted as a function of the crystal size L.

4.2.4 Deformation of the skyrmion configuration by magnetic field

In a single-skyrmion approach, the isolated-skyrmion configuration is deformed by a magnetic field, as discussed in [44]. In the skyrmion crystal approach a magnetic field distorts the skyrmion crystal configuration. In this subsection we discuss the deformation of the skyrmion configuration and the single-baryon shape under a magnetic field.

In the skyrmion crystal approach, the magnetic contribution to the skyrmion crystal configuration can be described by plotting the baryon-

number density-distribution functions in Eq.(4.13). Notice that even without a magnetic field, the skyrmion configurations differ between in the skyrmon phase and the half-skyrmion phase because of the different crystal forms (FCC and CC) triggered by the topological phase transition, as shown in Sec. 3.4.2. One can easily find that for the winding number term $\rho_W(x,y,z)$ in Eq.(4.13) the crystal symmetries in the FCC and CC structures are still intact even in a magnetic field: for instance the translational symmetries are observed as

$$\begin{aligned}
&\text{skyrmion phase(FCC):}\\
&\rho_W(x,y,z) = \rho_W(x+L,y+L,z) = \rho_W(x+L,y,z+L)\\
&\qquad\qquad = \rho_W(x,y+L,z+L),\\
&\text{half-skyrmion phase(CC):}\\
&\rho_W(x,y,z) = \rho_W(x+L,y,z) = \rho_W(x,y+L,z) = \rho_W(x,y,z+L).
\end{aligned} \tag{4.18}$$

The winding number density takes the form of the intrinsic structure of the skyrmion crystal, which is obviously present in the absence of a magnetic field. On the other hand, for the induced-baryon number density $\tilde{\rho}_{eB}$ in Eq.(4.13) the crystal symmetries are explicitly broken by a magnetic field as

$$\begin{aligned}
&\text{skyrmion phase(FCC):}\\
&\tilde{\rho}_{eB}(x,y,z) = \tilde{\rho}_{eB}(x+L,y+L,z) = -\tilde{\rho}_{eB}(x+L,y,z+L)\\
&\qquad\qquad = -\tilde{\rho}_{eB}(x,y+L,z+L),\\
&\text{half-skyrmion phase(CC):}\\
&\tilde{\rho}_{eB}(x,y,z) = -\tilde{\rho}_{eB}(x+L,y,z) = -\tilde{\rho}_{eB}(x,y+L,z) = \tilde{\rho}_{eB}(x,y,z+L).
\end{aligned} \tag{4.19}$$

This implies that the presence of the induced-baryon number density would drastically deform the skyrmion configurations for both phases.

In Figs. 4.10, 4.11 and 4.12, we monitor the skyrmion crystal configurations in the skyrmion phase (in a low density region). First, it is a striking observation that the FCC structure essentially keeps even for a strong magnetic field region, as depicted in Fig. 4.12 for $\sqrt{eB} = 800$[MeV]. Looking at the single baryon shape as depicted in Figs. 4.10, 4.11 and 4.12, one can also find that the baryon shape is deformed to be like an elliptic shape, as $\sqrt{eB}$ gets larger. This behavior of the magnetic deformation has also been found in the isolated-skyrmion based on a single-skyrmion approach [44].

Moving on to the half-skyrmion phase (at a high density region), the skyrmion configurations are described in Figs. 4.13, 4.14 and 4.15. At the first glance, one immediately finds that the CC configuration, formed in the case without eB(Figs. 4.13), gets dramatically distorted, as $\sqrt{eB}$ increases.

Furthermore, in a strong magnetic field region where $\sqrt{eB} = 800$MeV, the x-z plane configurations imply that the strong magnetic effect makes a multiple-peak structure for the skyrmion configuration (see Fig.4.15). Of interest is also that in a strong magnetic field region a FCC-like structure has been created in the x-y plane configurations ((a) and (c) panels of Fig. 4.15). Those remarkable deformations in the half-skyrmion phase would be expected to be indirect probes for the certain evidence of the inhomogeneous chiral condensate as shown in Fig.4.7.

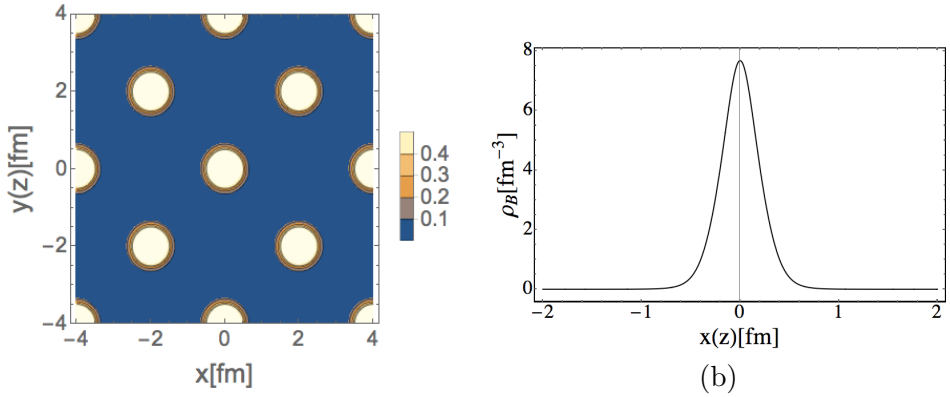

(a) (b)

Figure 4.10: The skyrmion configurations at $\sqrt{eB} = 0$ MeV and $L = 2.0$ fm (in the skyrmion phase). (a): x-y(z) plane. (b): x-axis specified at $y = z = 0$.

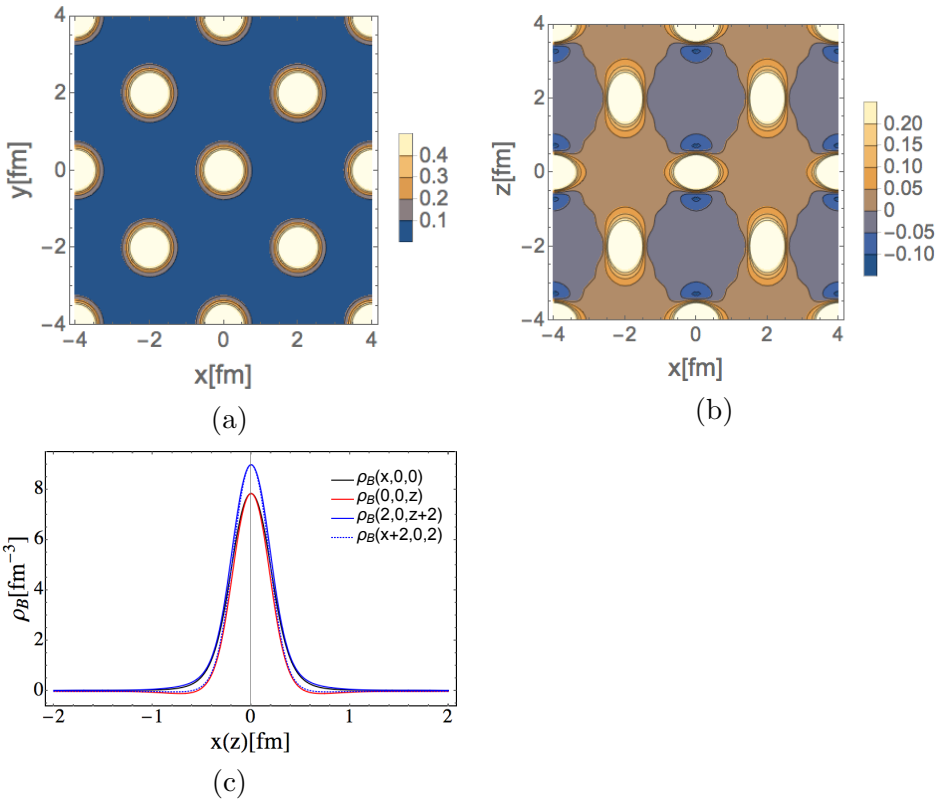

Figure 4.11: The skyrmion configurations with $\sqrt{eB} = 400$ MeV at $L = 2.0$ fm (in the skyrmion phase). (a): x-y plane. (b): x-z plane. (c): x-axis or z-axis including the size of shift by $L = 2.0$ fm.

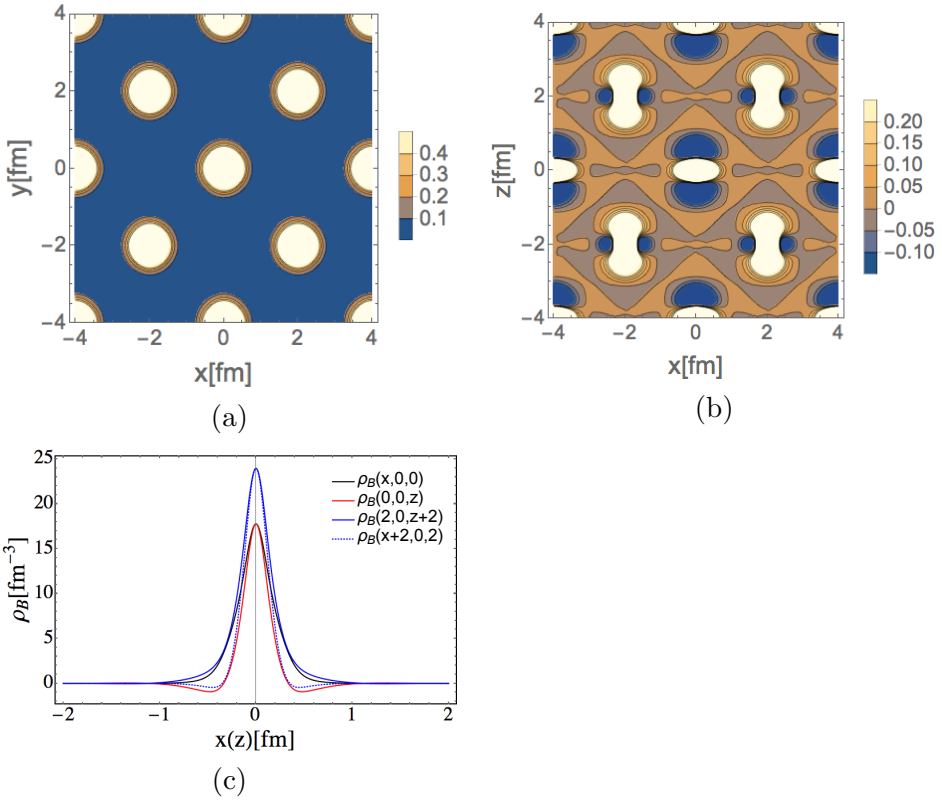

Figure 4.12: The skyrmion configurations with $\sqrt{eB} = 800$ MeV at $L = 2.0$ fm (in the skyrmion phase). (a): x-y plane. (b): x-z plane. (c): x-axis or z-axis including the size of shift by $L = 2.0$ fm.

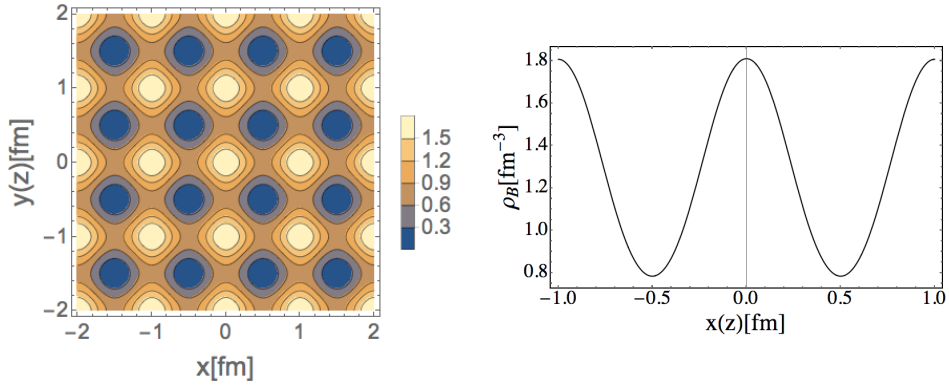

Figure 4.13: The skyrmion configurations with $\sqrt{eB} = 0$ MeV at $L = 1.0$ fm (in the half-skyrmion phase). (a): x-y(z) plane. (b): x-axis specified at $y = z = 0$.

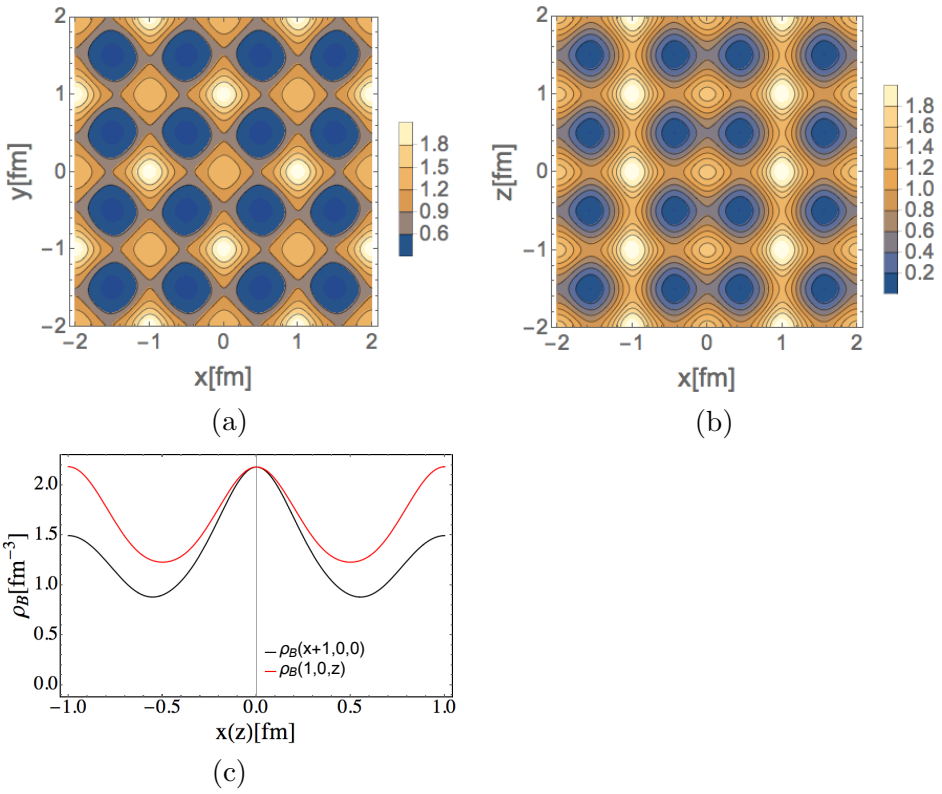

Figure 4.14: The skyrmion configurations with $\sqrt{eB} = 400$ MeV at $L = 1.0$ fm (in the half-skyrmion phase). (a): x-y plane. (b): x-z plane. (c): x-axis or z-axis including the size of shift by $L = 1.0$ fm .

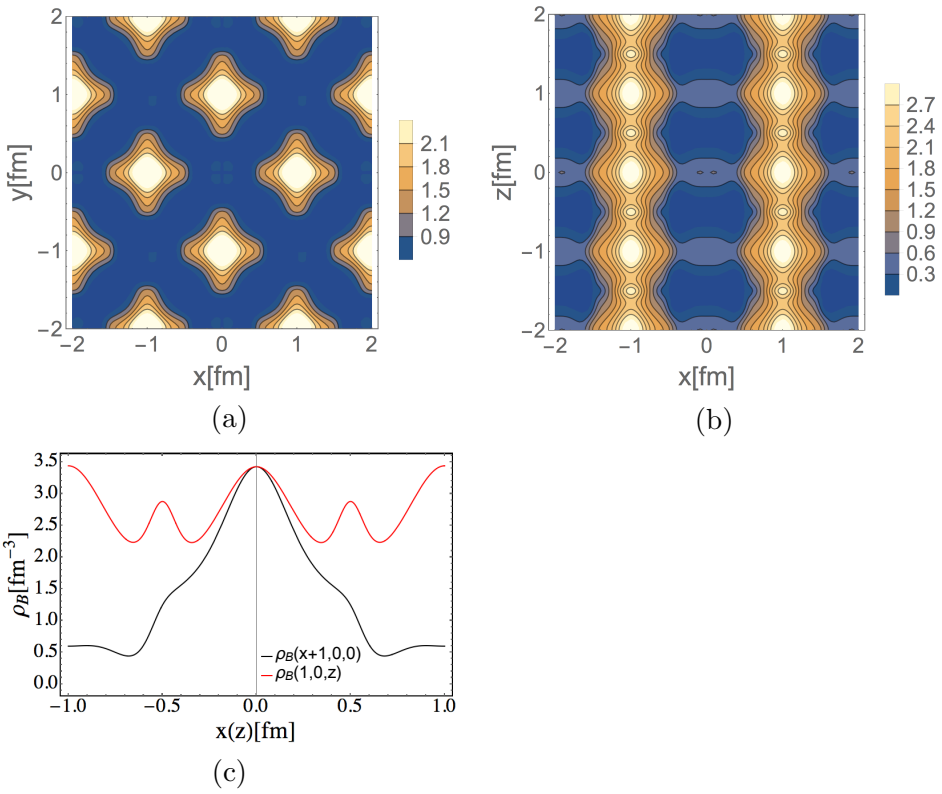

Figure 4.15: The skyrmion configurations with $\sqrt{eB} = 800$ MeV at $L = 1.0$ fm (in the half-skyrmion phase). (a): x-y plane. (b): x-z plane. (c): x-axis or z-axis including the size of shift by $L = 1.0$ fm .

Chapter 5

Conclusion

We have analyzed the magnetic properties of a baryonic matter based on the skyrmion crystal model. What we have observed throughout this thesis are as follows.

The per-baryon energy (Skyrme energy) is enhanced by a magnetic field for any crystal size (any density region). The magnetic dependence on the Skyrme energy is restricted by the crystal configuration (crystal symmetry), so that in low density region this magnetic dependence is not like the one as seen in the isolated skyrmion case, which is thought as to be the intrinsic multi-body effect due to the crystal formation.

It has been also found that the magnetic effect tends to shift the topological phase transition point to a high density region. This behavior indicates that a magnetic field acts as a catalyzer for the topological phase transition. Furthermore, through analyzing the magnetic dependence on the inhomogeneous distribution of the chiral condensate, we found that even in the presence of a magnetic field the inhomogeneity for the chiral condensate persists both in skyrmion and half-skyrmion phases. Remarkably enough, as the strength of a magnetic field increases, the inhomogeneous chiral condensate in the skyrmion phase is susceptible to be localized, while in the half-skyrmion phase the inhomogeneous distribution is negligibly affected as opposed to the skyrmion phase.

Through investigation of the magnetic effect on the skyrmion crystal configuration and the single-baryon shape in the crystal, we observed that in a low density region (skyrmion phase) a strong magnetic effect deforms the single-baryon shape to be like an elliptic form, while the whole crystal configuration keeps up the intrinsic crystal structure which is present in null magnetic environment. In a high density region (half-skyrmion phase), it was further shown that the CC crystal structure is completely spoiled by a strong magnetic field. In particular, by zooming in the x-y plane for a strong magnetic field region, even in the half-skyrmion phase the CC configuration effectively returns back to the original crystal structure as a FCC.

Based on the above consideration, a possible correlation between the inhomogeneity of chiral condensate and the deformation of the skyrmion crystal configuration was made: we observed that a nontrivial deformation is correlated with the chiral inhomogeneity by a strong magnetic field. It would be expected that through this correlation we would indirectly confirm the presence of the inhomogeneity of the chiral condensate in the half-skyrmion phase.

Though quantitative predictions in the skyrmion crystal approach might be somewhat deviated from the realistic situation of nuclear matter, the magnetic behavior involving the magnetic catalysis would qualitatively be extracted as the essential properties of the high-dense baryonic matter. Furthermore, in the core of magnetars, a strong magnetic field might emerge, as was discussed along with a crucial correlation with the chiral dynamics in [52, 53]. Thus, the equation of state for the neutron stars based on the skyrmion crystal approach, as discussed in [54, 55, 56], should be affected by a magnetic field, so that the remnant of the topology transition in neutron stars and magnetars is also affected by a magnetic field.

Before closing this thesis, we shall make some comments on another intriguing aspect for the application of the skyrmion crystal model. Among such other topics, especially, let us take a look at the pion condensation in a baryonic matter. The pion condensation is expected to be realized in high dense baryonic matter, which is described as a periodic and parity-violating topological soliton. This pion condensation is more generically called chiral soliton lattice (CSL). Actually, in the condensed matter systems, the CSL has been investigated in chiral magnets [57] and the structure of CSL was observed in the recent experiment for chiral magnets [58]. Motivated by this fact, some attempts have been made to adapt the idea of CSL to QCD in terms of high energy system [52, 53, 59, 60]. Adapting the skyrmion crystal approach, the author in this thesis have investigated the CSL effect on the baryonic matter. It turns out that the presence of the CSL causes the topological phase transition point to shift to a low density region [61]. Furthermore, it has been found that the CSL makes the single-baryon shape deformed to be the oscillating object. Also, the things clarified by the study in [61] might deepen our understanding of compact stars.

Thus, as has been addressed so far throughout this thesis, the skyrmion crystal approach is powerful enough to investigate a new insight for the role of the chiral symmetry in dense matter with some external background such as a magnetic field, hence would certainly shed the light on a novel way of understanding for the QCD phase structure.

Acknowledgement

First and foremost I would like to deeply thank Professor Shinya Matsuzaki for the patient guidance, encouragement and helpful advice. I have been extremely lucky to have such a supervisor who cared so much about my work, and responded to my questions and queries so promptly. I am also very grateful to Professor Masayasu Harada and Professor Chiho Nonaka. Valuable advice and insightful comments given by them has been a great help in my research. I appreciate Professor Yong-Liang Ma for collaboration on the early stages of this work. I must express my gratitude to Professor Deog-Ki Hong for giving me a chance to stay and study at his group in Pusan National University. I really enjoyed everything during the stay. I am thankful to Yoshiki Kuroda, Yuki Shimizu, Yo-hei Kawakami and Takahiro Yamazaki for their supports in my research life and sharing precious time.

The work of M. K. is supported in part by JSPS Grant- in-Aid for JSPS Research Fellow No. 18J15329.

Appendix A

Non-linear realization

Here we discuss the non-linear realization for the spontaneous breaking of the chiral symmetry.

We first consider the general case in which the symmetry of the (Lie) group, G with the algebra $\mathcal{G}$, is spontaneously broken to its subgroup, H with the sub-algebra $\mathcal{H}$. Let T^A be a generator of $\mathcal{G}$ and $S^a\,(X^\alpha)$ be the unbroken (broken) generator in $\mathcal{H}$:

$$T^A \in \mathcal{G}, \;\; S^a \in \mathcal{H}, \;\; X^\alpha \in \mathcal{G} - \mathcal{H}. \tag{A.1}$$

These generators satisfy the following conditions,

$$\begin{aligned} [T^A, T^B] &= i f^{ABC} T^C, \quad [S^a, S^b] = i f^{abc} S^c, \\ \mathrm{tr}(T^A T^B) &= \frac{1}{2}\delta^{AB}, \qquad \mathrm{tr}(S^a S^b) = \frac{1}{2}\delta^{ab}, \\ \mathrm{tr}(X^\alpha X^\beta) &= \frac{1}{2}\delta^{\alpha\beta}, \qquad \mathrm{tr}(S^a X^\beta) = 0. \end{aligned} \tag{A.2}$$

By using Eq.(A.2), one can derive the trace product of $S^a[S^b, X^\alpha]$,

$$\mathrm{tr}(S^a[S^b, X^\alpha]) = \mathrm{tr}([S^a, S^b]X^\alpha) = 0. \tag{A.3}$$

This equation implies that the commutation relation between the unbroken generator S^a and the broken generator X^α takes the value as the algebra $\mathcal{G} - \mathcal{H}$ belonging to $G - H$, namely,

$$[S^a, X^\alpha] \in \mathcal{G} - \mathcal{H}. \tag{A.4}$$

In general the commutation relation between the broken generators $[X^\alpha, X^\beta]$ can be written as the linear combination of the the unbroken generator S^a and the broken generator X^α. For convenience, we specify the following condition,

$$[X^\alpha, X^\beta] \in \mathcal{H}. \tag{A.5}$$

Actually, in the case of the chiral symmetry the above condition is satisfied. Now one can find that the commutation relations in Eqs.(A.2, A.4, A.5) are invariant under the transformation τ,

$$\begin{cases} \tau(S) = +S & S \in \mathcal{H} \\ \tau(X) = -X & X \in \mathcal{G} - \mathcal{H} \end{cases} \tag{A.6}$$

$$\tau^2 = 1. \tag{A.7}$$

This implies that the transformation τ corresponds to the parity transformation.

Let g be the elements of G. The space of G can be decomposed into the joint of sets of $\{gH\}$ which corresponds to the left coset classes:

$$G = [H \cdot 1] \oplus [Hg_1] \oplus [Hg_2] \oplus \cdots , \tag{A.8}$$

where $[Hg]$ is the equivalent classes of the Hg. (The Hg is the representative for the equivalent classes, $[Hg]$.) Thus, the coset space, G/H, can be expressed as

$$G/H = [1] \oplus [g_1] \oplus [g_2] + \cdots . \tag{A.9}$$

The representatives $g_1, g_2, \cdots$ lie in the space of the broken generators. Furthermore the number of broken symmetry generators is given as

$$\begin{aligned} &(\text{Number of broken symmetry generators}) \\ &= \dim[G] - \dim[H] = \dim[G/H]. \end{aligned} \tag{A.10}$$

Therefore, let the representative of the coset space G/H be ξ parametrized by the NG bosons,

$$\xi(\pi) = e^{i\pi/f_\pi}, \tag{A.11}$$

with $\pi = \pi^\alpha X^\alpha$. Under the parity transformation τ, the π field transform as

$$\tau(\pi) = -\pi. \tag{A.12}$$

Thus, NG boson field, π, has the odd-parity.

To get the transformation of $\xi(\pi)$ under the symmetry, G, the $\xi(\pi')$ is multiplied by the g,

$$\xi(\pi')g. \tag{A.13}$$

In general, $\xi(\pi')g$ is in the equivalence class of other representatives $\xi(\pi)$. Incidentally, by performing the transformation of the H, an element in the

equivalent classes $[\xi(\pi)]$ can be described as $h(\pi, g)\xi(\pi)$, where $h(\pi, g) \in H$. Thus, the $\xi(\pi')g$ can be equivalent to the $h(\pi, g)\xi(\pi)$:

$$h(\pi, g) \cdot \xi(\pi) = \xi(\pi') \cdot g. \tag{A.14}$$

From this result the transformation of $\xi(\pi)$ under the symmetry, G, is given as

$$\xi(\pi) \to h(\pi, g)\xi(\pi)g^\dagger. \tag{A.15}$$

To construct the Lagrangian based on the nonlinear realization, we introduce the Maurer-Cartan1-form. By using the ξ, the Maurer-Cartan1-form is constructed as

$$\begin{aligned} \alpha_\mu(\pi) &= \frac{1}{i}\partial_\mu \xi(\pi) \cdot \xi^{-1}(\pi) \\ &= \frac{1}{i}\left(\frac{i}{f_\pi}\partial_\mu \pi + \frac{i^2}{2f_\pi^2}[\pi, \partial_\mu \pi] + \cdots\right). \end{aligned} \tag{A.16}$$

Note that terms including odd (even) number of the π fields corresponds to odd (even)-parity terms. Under the transformation of the symmetry G, the Maurer-Cartan 1-form transforms as

$$\alpha_\mu(\pi) \to h(\pi, g)\alpha_\mu(\pi)h^\dagger(\pi, g) + \frac{1}{i}\partial_\mu h(\pi, g) \cdot h^\dagger(\pi, g). \tag{A.17}$$

Here $\frac{1}{i}\partial_\mu h(\pi, g) \cdot h^\dagger(\pi, g)$ term lies in $\mathcal{H}$. To construct the G-invariant Lagrangian, this Maurer-Cartan1-form should be decomposed into the $\alpha_{||\mu} \in \mathcal{H}$ and $\alpha_{\perp\mu} \in \mathcal{G} - \mathcal{H}$,

$$\begin{aligned} \alpha_{||\mu} &\equiv \alpha_\mu^a S^a \\ \alpha_{\perp\mu} &\equiv \alpha_\mu^\alpha X^\alpha. \end{aligned} \tag{A.18}$$

The $\alpha_{||\mu}$ and $\alpha_{\perp\mu}$ transform as

$$\begin{aligned} \alpha_{||\mu} &\to h(\pi, g)\alpha_{||\mu}h^\dagger(\pi, g) - i\partial_\mu h(\pi, g) \cdot h^\dagger(\pi, g) \\ \alpha_{\perp\mu} &\to h(\pi, g)\alpha_{\perp\mu}h^\dagger(\pi, g). \end{aligned} \tag{A.19}$$

Now we consider the case of the chiral $G = SU(2)_L \times SU(2)_R$ symmetry spontaneously broken to the $H = SU(2)_V$. Let $g_{L,R}$ be the elements of the chiral symmetry, $g_{L,R} \in SU(2)_{L,R}$, and write the transformation matrix for $g_{L,R}$ as

$$\begin{aligned} g_R &= \exp[i\theta_R^a \tau^a] = \exp[i(\theta_V^a + \theta_A^a)\tau^a] \\ g_L &= \exp[i\theta_L^a \tau^a] = \exp[i(\theta_V^a - \theta_A^a)\tau^a]. \end{aligned} \tag{A.20}$$

The unbroken charge corresponds to the vector charge Q_V^a which is associated with the vector transformation with $g_R = \exp(i\theta_V^a \tau^a)$ and $g_L =$

$\exp(i\theta_V^a\tau^a)$. On the other hand, the axial charge Q_A^a denotes the broken charge, which is related to the axial transformation with $g_R = \exp(i\theta_A^a\tau^a)$ and $g_L = \exp(-i\theta_A^a\tau^a)$. This indicates that the representatives of the coset space in the case of the chiral symmetry is described as

$$\xi_{L,R} = e^{\mp i\pi^\alpha X^\alpha/f_\pi}. \tag{A.21}$$

Under the chiral symmetry, the $\xi_{L,R}$ transforms as

$$\xi_{L,R} \to h(\pi, g_L, g_R)\xi_{L,R}g_{L,R}^\dagger. \tag{A.22}$$

By using Eq.(A.21), the Maurer-Cartan 1-form for the chiral symmetry is constructed as,

$$\begin{aligned} \alpha_{||\mu} &= \frac{1}{2i}(\partial_\mu\xi_R\cdot\xi_R^\dagger + \partial_\mu\xi_L\cdot\xi_L^\dagger) \in \mathcal{H} \\ \alpha_{\perp\mu} &= \frac{1}{2i}(\partial_\mu\xi_R\cdot\xi_R^\dagger - \partial_\mu\xi_L\cdot\xi_L^\dagger) \in \mathcal{G}-\mathcal{H}. \end{aligned} \tag{A.23}$$

The $\alpha_{||\mu}$ and $\alpha_{\perp\mu}$ transform as

$$\begin{aligned} \alpha_{||\mu} &\to h(\pi, g_L, g_R)\alpha_{||\mu}h^\dagger(\pi, g_L, g_R) - i\partial_\mu h(\pi, g_L, g_R)\cdot h^\dagger(\pi, g_L, g_R) \\ \alpha_{\perp\mu} &\to h(\pi, g_L, g_R)\alpha_{\perp\mu}h^\dagger(\pi, g_L, g_R). \end{aligned} \tag{A.24}$$

The $\alpha_{\perp\mu}$ transforms homogeneously. In the general way, the chiral invariant Lagrangian (at the leading order of the derivative couplings) is thus written by using only the $\alpha_{\perp\mu}$ as

$$\mathcal{L} = F_\pi^2\mathrm{tr}[\alpha_{\perp_\mu}\alpha_\perp^\mu]. \tag{A.25}$$

By using the $\xi_{L,R}$, the chiral field U is expressed as

$$U = \xi_L^\dagger\xi_R. \tag{A.26}$$

The perpendicular component of the Maurer-Cartan 1-form can then be written as

$$\alpha_{\perp\mu} = \frac{1}{2i}\xi_L(\partial_\mu U)\xi_R^\dagger. \tag{A.27}$$

Thus, the Lagrangian in Eq.(A.25) is equivalent to the chiral Lagrangian as seen in Eq.(2.36) :

$$\mathcal{L} = F_\pi^2\mathrm{tr}[\alpha_{\perp_\mu}\alpha_\perp^\mu] = \frac{F_\pi^2}{4}\mathrm{tr}[\partial_\mu U\partial^\mu U^\dagger]. \tag{A.28}$$

Appendix B

Large N_C expansion

The large N_c expansion is a powerful tool to evaluate the nonperturbative QCD in a systematic way. In this appendix, we briefly review the large N_c expansion.

For a gauge theory with color gauge group $SU(N_c)$ coupled to the N_f number of fermions, and the gauge coupling g, the $g^2 N_c$ is kept fixed in the limit $N_c \to \infty$, as was pointed by 't Hooft, [62]. At the one-loop level, the running coupling constant renormalized at the scale μ, $g(\mu)$, is evaluated as

$$\frac{g^2(\mu)}{(4\pi)^2} = \frac{1}{\beta_0 \ln(\mu^2/\Lambda^2_{\rm QCD})}, \quad \beta_0 = \frac{1}{3}(11N_c - 2N_f), \tag{B.1}$$

where $\Lambda_{\rm QCD}$ is the typical mass scale in QCD ($\Lambda_{\rm QCD}$ does not denote an ultraviolet cutoff). This implies that in the large N_c limit the running coupling constant goes to zero, and then the g^2 can be assigned to

$$g^2 \sim \frac{1}{N_c}. \tag{B.2}$$

Therefore, in the large N_c limit we can expand the Green functions of the $SU(N_c)$ gauge theory in the powers of $1/N_c$.

To consider the large N_c expansion for the effective action of the $SU(N_c)$ gauge theory, we shall introduce the external fields into the QCD Lagrangian,

$$\mathcal{L}_{\rm QCD} = \mathcal{L}^0_{QCD} + \bar{q}\gamma^\mu(\mathcal{V}_\mu + \gamma_5 \mathcal{A}_\mu)q + \bar{q}(S + i\gamma_5 P)q, \tag{B.3}$$

where $\mathcal{L}^0_{\rm QCD}$ is the ordinary QCD Lagrangian and $\mathcal{V}_\mu$, $\mathcal{A}_\mu$, S and P are the external fields. Note that the quark and gluon fields belong to the fundamental and adjoint representations, respectively, so that the one loop diagram of quark (gluon) has a factor of N_c (N_c^2). Then it is expected that the leading order of the effective action is of $\mathcal{O}(N_c^2)$.

The low energy theory can be connected to QCD through the generating function. The Green functions of currents are generated by differentiating

the generating function with the external fields:

$$\langle 0|Tj^i_{V\mu}(x)j^j_{A\nu}(y)\cdots|0\rangle = \frac{1}{Z^0_{\rm QCD}}\left(\frac{\delta}{\delta\mathcal{V}^i_\mu}\frac{\delta}{\delta\mathcal{A}^j_\nu}\cdots\right)Z_{\rm QCD}\Big|_{\mathcal{V}_\mu=\mathcal{A}_\mu=S=P=0}, \tag{B.4}$$

where

$$Z_{\rm QCD}[\mathcal{V}_\mu,\mathcal{A}_\mu,S,P] = \int[dq]\,[d\bar{q}]\,[dG]\,\exp\left(i\int d^4x\mathcal{L}_{\rm QCD}\right), \tag{B.5}$$

with $Z^0_{\rm QCD} = Z_{\rm QCD}[0,0,0,0]$. In the low energy region, the Green functions can be reproduced by using the effective Lagrangian $\mathcal{L}_{\rm eff}$, which is consist with the chiral symmetry:

$$\langle 0|Tj^i_{V\mu}(x)j^j_{A\nu}(y)\cdots|0\rangle = \frac{1}{Z_0}\left(\frac{\delta}{\delta\mathcal{V}^i_\mu}\frac{\delta}{\delta\mathcal{A}^j_\nu}\cdots\right)Z_{\rm eff}\Big|_{\mathcal{V}_\mu=\mathcal{A}_\mu=S=P=0}, \tag{B.6}$$

where

$$Z_{\rm eff}[\mathcal{V}_\mu,\mathcal{A}_\mu,S,P] = \int[d\sigma]\,[d\pi]\,[\cdots]\exp\left(i\int d^4x\mathcal{L}_{\rm eff}\right), \tag{B.7}$$

with $Z^0_{\rm eff} = Z_{\rm eff}[0,0,0,0]$. Namely, through the generating function, the low energy effective theory can be connected to QCD: $Z_{\rm QCD} = Z_{\rm eff}$. In this sense, the Large N_c counting can be adapted to the low energy effective theory.

First, we investigate the N_c counting for the pion mass and the pion decay constant through the correlation function of the axial current,

$$\langle 0|Tj^i_{A\mu}(x)j^j_{A\nu}(y)|0\rangle. \tag{B.8}$$

From the QCD Lagrangian, the axial current is denoted as $j^i_{A\mu} = \bar{q}\gamma_\mu\gamma_5\tau^i q$, so that the leading contribution to this correlation function is of $\mathcal{O}(N_c)$:

$$\langle 0|Tj^i_{A\mu}(x)j^j_{A\nu}(y)|0\rangle = -N_c\delta^{ij}{\rm tr}[D(y-x)\gamma_\mu\gamma_5 D(x-y)\gamma_\nu\gamma_5] + \cdots, \tag{B.9}$$

where $D(x)$ denotes the quark propagator. On the other hand, in the low energy region the axial current can be estimated as $j^i_{A\mu} = f_\pi\partial_\mu\pi^i + \cdots$ (see Eq.(2.27)). Using this current form, the correlation function is expressed as

$$\langle 0|Tj^i_{A\mu}(x)j^j_{A\nu}(y)|0\rangle = f_\pi^2\int\frac{d^4p}{(2\pi)^4}\frac{ip_\mu p_\nu}{p^2-m_\pi^2}e^{-ip\cdot(x-y)} + \cdots. \tag{B.10}$$

The momentum of the pion does not have the color number, $p\sim\mathcal{O}(1)$, so that pion mass is of $\mathcal{O}(1)$,

$$m_\pi \sim \mathcal{O}(1). \tag{B.11}$$

Since the left hand side in Eq.(B.10) is of $\mathcal{O}(N_c)$, the pion decay constant can be assigned as

$$f_\pi \sim \mathcal{O}(\sqrt{N_c}). \tag{B.12}$$

Next we explore the coupling constant of the meson interaction. As a sample, we shall take the Skyrme model and the Skyrme term as in Eq.(4.2),

$$\begin{aligned} & \frac{1}{(32 g_{\rm Skyr}^2)} {\rm tr}\Big([U^\dagger \partial_\mu U, U^\dagger \partial_\nu U][U^\dagger \partial^\mu U, U^\dagger \partial^\nu U] \Big) \\ = & -\frac{1}{4 g_{\rm Skyr}^2 f_\pi^4} (\delta^{ac}\delta^{bd} - \delta^{ad}\delta^{bc}) \partial_\mu \pi^a \partial_\nu \pi^b \partial^\mu \pi^c \partial^\nu \pi^d + \cdots . \end{aligned} \tag{B.13}$$

In the Skyrme term, the trace product amounts to a sum over the flavors of quarks, so that the single trace product corresponds to the one loop calculation of quark in the 4-point correlation function of the axial current:

$$\langle 0 | T j^i_{A\mu}(x) j^j_{A\nu}(y) j^k_{A\rho}(z) j^l_{A\nu}(w) | 0 \rangle \sim \mathcal{O}(N_c). \tag{B.14}$$

On the other hand, in the low energy region the 4-point correlation function of the axial current is evaluated by using the interaction Eq.(B.13),

$$\begin{aligned} & \langle 0 | T j^i_{A\mu}(x) j^j_{A\nu}(y) j^k_{A\rho}(z) j^l_{A\nu}(w) | 0 \rangle \\ & = (f_\pi)^4 \langle 0 | T \partial_\mu \pi^i(x) \partial_\nu \pi^j(y) \partial_\rho \pi^k(z) \partial_\sigma \pi^l(w) \\ & \times \int d^4x' \left(-\frac{1}{4 g_{\rm Skyr}^2 f_\pi^4} \right) (\delta^{ac}\delta^{bd} - \delta^{ad}\delta^{bc}) \partial_{\mu'} \pi^a \partial_{\nu'} \pi^b \partial^{\mu'} \pi^c \partial^{\nu'} \pi^d (x') | 0 \rangle + \cdots \\ & \sim \left(-\frac{1}{4 g_{\rm Skyr}^2} \right) \times (\text{function of pion propagators}) + \cdots . \end{aligned} \tag{B.15}$$

Thus, one concludes that

$$g_{\rm Skyr} \sim \mathcal{O}(1/\sqrt{N_c}). \tag{B.16}$$

Finally, we comment on the N_c counting for baryons. For the $SU(N_c)$ gauge theory, a baryon arises as a completely anti-symmetric state under interchanges of N_c quarks. In the quark model picture, the baryon mass, m_N, might be expressed as

$$m_N = N_c m_q + N_c T + V, \tag{B.17}$$

where m_q is the quark mass counted as $\mathcal{O}(N_c^0)$, T denotes the kinetic energy of single quark, which is of $\mathcal{O}(N_c^0)$, and V represents the potential energy of quark-quark interactions. The simplest potential energy is expressed as the one gluon exchange between one pair of quarks. Since there are N_c

quarks in a single baryon, the number of the combination factor amounts to $(N_c^2-1)/2$. The potential is thus proportional to $(N_c^2-1)/2$ and g^2,

$$V = \frac{N_c^2-1}{2} g^2 \bar{V}_1, \tag{B.18}$$

where $\bar{V}_1$ is the rest of the potential energy after the g^2 factor is extracted, hence counted as $\mathcal{O}(N_c^0)$ in the large N_c expansion. By the large N_c expansion, the baryon mass is then

$$\begin{aligned} m_N &= N_c m_q + N_c T + \frac{N_c^2-1}{2} g^2 \bar{V}_1 \\ &\sim N_c (m_q + T + \bar{V}_1). \end{aligned} \tag{B.19}$$

Thus, the baryon mass is of order N_c,

$$m_N \sim \mathcal{O}(N_c). \tag{B.20}$$

Actually, the baryon dynamics can be viewed as a many-body system in terms of N_f quarks, hence can be described by using the time-independent Schrodinger equation for the many-body wavefunction $\psi(x_1, x_2, \cdots, x_{N_c})$,

$$\psi(x_1, \cdots, x_{N_c}) = \prod_{i=1}^{N_c} \phi(x_i), \tag{B.21}$$

where ϕ is the normalized wave function of a single-quark. Through the analysis of the many body problem in terms of quarks we can thus discuss the large N_c scaling for the charge radius of baryons.

For the baryon in the $SU(N_c)$ gauge theory, we have a non-relativistic Hamiltonian operator like

$$H = N_c m_q + N_c \frac{-\partial^2}{2m_q} - \frac{N_c^2-1}{2} \cdot \frac{g_{\rm eff}^2}{N_c} \frac{1}{|\vec{x}_1 - \vec{x}_2|}, \tag{B.22}$$

with $g_{\rm eff} \sim \sqrt{N_c} g \sim \mathcal{O}(1)$. The time-independent Schrodinger equation can be derived from the variational principle method. Then, by using the Hamiltonian, the variational function for the many-body quark system, $\langle \psi | H - E | \psi \rangle$, is calculated as

$$\begin{aligned} \langle \psi | H - E | \psi \rangle &= N_c m_q + \frac{N_c}{2m_q} \sum_{i=1}^{N_c} \int d^3x_i \partial\phi^*(x_i) \partial\phi(x_i) \\ &\quad - \frac{N_c^2-1}{2} \cdot \frac{g_{\rm eff}^2}{N_c} \int d^3x_1 \int d^3x_2 \frac{|\phi(x_1)|^2 |\phi(x_2)|^2}{|\vec{x}_1 - \vec{x}_2|} - E. \\ &= N_c \Bigg(m_q + \frac{1}{2m_q} \sum_{i=1}^{N_c} \int d^3x_i \partial\phi^*(x_i) \partial\phi(x_i) \\ &\quad - \frac{g_{\rm eff}^2}{2} \int d^3x_1 \int d^3x_2 \frac{|\phi(x_1)|^2 |\phi(x_2)|^2}{|\vec{x}_1 - \vec{x}_2|} - \epsilon \prod_{i=1}^{N_c} \int d^3x_i |\phi(x_i)|^2 \Bigg), \end{aligned}$$

where E is written as $E = N_c\epsilon$ with ϵ being the energy per quark. From this variational function, the Schrodinger equation reads

$$-\frac{\partial^2}{2M}\phi(x_i) - g_{\rm eff}^2\phi(x_i)\int d^3x_1 \frac{|\phi(x_1)|^2}{|\vec{x}_1 - \vec{x}_i|} = \epsilon\phi(x_i). \tag{B.23}$$

From this equation, we see that the quark wavefunction ϕ does not depend on N_c, neither do the baryon wavefunction ψ. Thus, the charge radius of baryon, $\langle r^2\rangle$, is of order $\mathcal{O}(1)$:

$$\langle r^2\rangle = \langle\psi|r^2|\psi\rangle \sim \mathcal{O}(1). \tag{B.24}$$

As for the baryon-baryon scattering, we can observe that one quark jumps from each baryon to the other baryon through the one gluon exchange. Then, the contribution of the one gluon exchange is proportional to $N_c^2 g^2$, so that the amplitude of the baryon-baryon scattering is of $\mathcal{O}(N_c)$.

Appendix C

Quantization for skyrmion

The skyrmion can be quantized to be endowed with spin and isospin quantum numbers. In this appendix, we discuss the quantization for the skyrmoin.

To quantize the skyrmion, we may rotate the classical solution by an $SU(2)$ isospin transformation,

$$U(\boldsymbol{x},t) = A(t)U_c(\boldsymbol{x})A^\dagger(t), \tag{C.1}$$

where U_c is the classical solution of the skyrmion and $A(t)$ is a time-dependent $SU(2)$ matrix. By using three parameters $\theta_i(t)$ the $SU(2)$ rotation matrix $A(t)$ can be written as

$$A(t) = \exp\bigl(i\boldsymbol{\tau}\cdot\boldsymbol{\theta}(t)\bigr) = \mathbf{1_{2\times 2}}\cdot\cos\theta(t) + i\frac{\boldsymbol{\tau}\cdot\boldsymbol{\theta}(t)}{\sqrt{\theta^2(t)}}\sin\theta(t). \tag{C.2}$$

This matrix takes the form like

$$A(t) = a_0\cdot 1_{\mathbf{2\times 2}} + i\tau^i a^i, \tag{C.3}$$

where $A(t)$ satisfies the unitary condition, $\sum_{\alpha=0}^{3} a_\alpha^2{=}1$ for the expansion parameters a_α.

For convenience, we introduce the angular velocity Ω_i in such a way that

$$A^\dagger\partial_0 A = \frac{i}{2}\boldsymbol{\tau}\cdot\boldsymbol{\Omega}, \tag{C.4}$$

where

$$\Omega^i = 2(\partial_0 a_0\cdot a_i - a_0\partial_0 a_i + f^{ijk}a_j\partial_0 a_k). \tag{C.5}$$

By substituting Eqs.(C.1) and (C.4) into the Skyrme Lagrangian, the kinetic-term part reads

$$\begin{aligned} & \mathrm{tr}[\partial_\mu U(\boldsymbol{x},t)\partial^\mu U^\dagger(\boldsymbol{x},t)] \\ = \;& 2\left\{(\Omega^i)^2 - (\Omega^i\hat{x}^i)^2\right\}\sin^2 F - \mathrm{tr}[\partial_i U_c(\boldsymbol{x})\partial_i U_c^\dagger(\boldsymbol{x})], \end{aligned} \tag{C.6}$$

As for the Skyrme term, we have

$$\begin{aligned} & \mathrm{tr}\Big([U^\dagger\partial_\mu U, U^\dagger\partial_\nu U][U^\dagger\partial^\mu U, U^\dagger\partial^\nu U]\Big) \\ = \;& 16\left(\mathbf{\Omega}^2 - (\Omega^a\hat{x}^a)^2\right)\left\{(\partial_r F)^2 + \frac{\sin^2 F}{r^2}\right\}\sin^2 F \\ & + \mathrm{tr}\Big([U_c^\dagger\partial_i U_c, U_c^\dagger\partial_j U_c][U_c^\dagger\partial_i U_c, U_c^\dagger\partial_j U_c]\Big). \end{aligned} \tag{C.7}$$

Then, the time-dependent Lagrangian is obtained as

$$L_{\mathrm{Skyr}} = -\int d^3x\mathcal{L}_c + 2\mathcal{I}_{\mathrm{Skyr}}\left\{(\partial_0 a_0)^2 + (\partial_0 a_i)^2\right\}, \tag{C.8}$$

where $\mathcal{L}_c$ is described by the static classical solution of the skyrmion and the $\mathcal{I}_{\mathrm{Skyr}}$ is given by

$$\mathcal{I}_{\mathrm{Skyr}} = \frac{8\pi}{3}\int_0^\infty dr\, r^2\left[f_\pi^2 + \frac{1}{g^2}\left\{(\partial_r F)^2 + \frac{\sin^2 F}{r^2}\right\}\right]\sin^2 F. \tag{C.9}$$

After scaling $r \to r'/(gf_\pi)$, the $\mathcal{I}_{\mathrm{Skyr}}$ can be rewritten as

$$\mathcal{I}_{\mathrm{Skyr}} = \frac{1}{g^3 f_\pi}\frac{8\pi}{3}\int_0^\infty dr'\, r'^2\left[1 + (\partial_{r'} F)^2 + \frac{\sin^2 F}{r'^2}\right]\sin^2 F. \tag{C.10}$$

To find the Hamiltonian for the time-dependent Lagrangian, L_{Skyr}, the canonical momentum for a_i is introduced as

$$\pi_\alpha = \frac{\partial L_{\mathrm{Skyr}}}{\partial(\partial_0 a_\alpha)} = 4\mathcal{I}_{\mathrm{Skyr}}\partial_0 a_\alpha, \quad (\alpha = 0, 1, 2, 3). \tag{C.11}$$

Then, the Hamiltonian is given as

$$\begin{aligned} H_{\mathrm{Skyr}} &= \pi_\alpha\partial_0 a_\alpha - L_{\mathrm{Skyr}} \\ &= -\int d^3x\mathcal{L}_c + \frac{1}{8\mathcal{I}_{\mathrm{Skyr}}}(\pi_\alpha)^2. \end{aligned} \tag{C.12}$$

To endow the skyrmion with spin and isospin quantum numbers, we shall adapt the canonical quantization conditions,

$$[a_\alpha, \pi_\beta] = i\delta_{\alpha\beta}. \tag{C.13}$$

Then, the canonical momenta is expressed by the differential operator as $\pi_i = -i\partial/\partial a_i$. The Hamiltonian operator thus reads

$$\hat{H}_{\mathrm{Skyr}} = -\int d^3x\mathcal{L}_c - \frac{1}{8\mathcal{I}_{\mathrm{Skyr}}}\sum_{\alpha=0}^{3}\left(\frac{\partial}{\partial a_\alpha}\right)^2. \tag{C.14}$$

To determine the eigenvalues and eigenvectors of $\hat{H}_{\rm Skyr}$, we focus on the familiar three dimensional Laplacian,

$$\sum_{i=1}^{3}\left(\frac{\partial}{\partial a_i}\right)^2 = \frac{\partial^2}{\partial r^2} + \frac{2}{r}\frac{\partial}{\partial r} - \frac{1}{r^2}\hat{\boldsymbol{L}}^2, \tag{C.15}$$

with $r = \sqrt{a_1^2 + a_2^2 + a_3^2}$. The $\hat{\mathbf{L}} = (L_1, L_2, L_3)^T$ are the angular momentum operators, which satisfy the algebra of $SO(3)$,

$$[L_i, L_j] = i\epsilon_{ijk}L_k. \tag{C.16}$$

These L_1, L_2 and L_3 operators generate rotations in the a_2-a_3, a_1-a_3 and a_1-a_2 planes, respectively. With the constraint condition, $r^2 = 1$, the three dimensional Laplacian is denoted by only the angular momentum $\boldsymbol{L}$,

$$\sum_{i=1}^{3}\left(\frac{\partial}{\partial a_i}\right)^2 = \hat{\boldsymbol{L}}^2. \tag{C.17}$$

We can adapt this analogy to the four dimensional laplacian. In the four dimension case, we should include the additional operators K_1, K_2, K_3 which generate rotations in the a_0-a_1, a_0-a_2 and a_0-a_3 planes, respectively. Thus the total six operators are denoted as

$$L_i = \epsilon_{ijk}a_j\pi_k, \quad K_i = a_0\pi_i - a_i\pi_0. \tag{C.18}$$

These operators form the $SO(4)$ symmetry group and the commutation relations read

$$[L_i, L_j] = i\epsilon_{ijk}L_k, \quad [L_i, K_j] = i\epsilon_{ijk}K_k, \quad [K_i, K_j] = i\epsilon_{ijk}L_k. \tag{C.19}$$

By introducing six operators

$$T_i = \frac{1}{2}(L_i - K_i), \quad J_i = \frac{1}{2}(L_i + K_i), \tag{C.20}$$

the commutation relations in the four dimension case are expressed as

$$[T_i, T_j] = i\epsilon_{ijk}T_k, \quad [T_i, J_j] = 0, \quad [J_i, J_j] = i\epsilon_{ijk}J_k. \tag{C.21}$$

The T_i and J_i satisfy the $SU(2)$ algebras respectively. We can associate the T_i and J_i with the isospin and the angular momentum (spin) respectively. The explicit expressions for the T_i and J_i are given as

$$\begin{aligned} T_i &= \frac{1}{2}(\epsilon_{ijk}a_j\pi_k - a_0\pi_i + a_i\pi_0) \\ &= \frac{-i}{2}\left(\epsilon_{ijk}a_j\frac{\partial}{\partial a_k} - a_0\frac{\partial}{\partial a_i} + a_i\frac{\partial}{\partial a_0}\right), \\ J_i &= \frac{1}{2}(\epsilon_{ijk}a_j\pi_k + a_0\pi_i - a_i\pi_0) \\ &= \frac{-i}{2}\left(\epsilon_{ijk}a_j\frac{\partial}{\partial a_k} + a_0\frac{\partial}{\partial a_i} - a_i\frac{\partial}{\partial a_0}\right). \end{aligned} \tag{C.22}$$

The T^2 and J^2 are actually set to the four-dimensional Laplacian as

$$T^2 = J^2 = -\frac{1}{4}\sum_{\alpha=0}^{3}\left(\frac{\partial}{\partial a_\alpha}\right)^2. \tag{C.23}$$

Here we have used the following relation,

$$\sum_{\alpha=0}^{3} a_\alpha \frac{\partial}{\partial a_\alpha} = 0. \tag{C.24}$$

By using the isospin and the angular momentum operators, T_i and J_i, the Hamiltonian operator can be written as

$$\begin{aligned}\hat{H}_{\rm Skyr} &= -\int d^3x \mathcal{L}_c + \frac{1}{4\mathcal{I}_{\rm Skyr}}(\boldsymbol{T}^2 + \boldsymbol{J}^2) \\ &= -\int d^3x \mathcal{L}_c + \frac{1}{2\mathcal{I}_{\rm Skyr}}\boldsymbol{J}^2. \end{aligned}\tag{C.25}$$

Then, the eigenvalue spectrum is expressed as

$$E_{\rm Skyr} = -\int d^3x \mathcal{L}_c + \frac{1}{2\mathcal{I}_{\rm Skyr}} J(J+1), \tag{C.26}$$

with $J = 0,\ 1/2,\ 1,\ 3/2, \cdots$. For the fermion, we take half-integer numbers for the J. The case of $J = 1/2$ corresponds to the eigenvalue spectrum of the proton and neutron.

The eigenstates for $T_3 = I_3 = 1/2$, which correspond to proton and neutrons with the up and down spins, are given as

$$\begin{aligned} |p\uparrow\rangle &= \frac{1}{\pi}(a_1 + ia_2), \quad |p\downarrow\rangle = -\frac{i}{\pi}(a_0 - ia_3), \\ |n\uparrow\rangle &= \frac{i}{\pi}(a_0 + ia_3), \quad |n\downarrow\rangle = -\frac{1}{\pi}(a_1 - ia_2). \end{aligned}\tag{C.27}$$

The normalization factor is obtained through integrating over the three-dimensional sphere:

$$\langle p\uparrow || p\uparrow\rangle = \frac{1}{\pi^2}\int d\Omega_3 (a_1^2 + a_2^1) = 1, \tag{C.28}$$

where

$$\int d\Omega_3 = \int_0^{2\pi} d\phi \int_0^{\pi} d\theta\, \sin\theta \int_0^{\pi} d\chi\, \sin^2\chi, \tag{C.29}$$

with the spherical coordinates being $a_1 = \sin\chi\sin\theta\cos\phi$, $a_2 = \sin\chi\sin\theta\sin\phi$, $a_3 = \sin\chi\cos\theta$, $a_4 = \cos\chi$. The notations for up- and down-signed spins with respect to the eigenstates are defined as follows:

$$\begin{aligned} &L_3|p\uparrow\rangle = +|p\uparrow\rangle, \quad K_3|p\uparrow\rangle = 0, \\ &L_3|p\downarrow\rangle = 0, \qquad\quad K_3|p\downarrow\rangle = -|p\downarrow\rangle, \\ &L_3|n\uparrow\rangle = 0, \qquad\quad K_3|n\uparrow\rangle = +|n\uparrow\rangle, \\ &L_3|n\downarrow\rangle = -|n\downarrow\rangle, \quad K_3|n\downarrow\rangle = 0. \end{aligned}\tag{C.30}$$

Appendix D

Wess-Zumino-Witten term

In the two-flavor case the explicit form of the Wess Zumino-Witten term is given by [63, 64],

$$
\begin{aligned}
\Gamma_{WZW} \;=\; & \frac{N_c}{48\pi^2}\int d^4x\epsilon^{\mu\nu\rho\sigma} \\
& \times\mathrm{tr}\Big[\mathcal{L}_\mu(\partial_\nu U\cdot U^\dagger)(\partial_\rho U\cdot U^\dagger)(\partial_\sigma U\cdot U^\dagger)+\mathcal{R}_\mu(U^\dagger\partial_\nu U)(U^\dagger\partial_\rho U)(U^\dagger\partial_\sigma U) \\
& +i(\mathcal{L}_\mu\partial_\nu\mathcal{L}_\rho+\partial_\mu\mathcal{L}_\nu\cdot\mathcal{L}_\rho)(\partial_\sigma U\cdot U^\dagger)+i(\mathcal{R}_\mu\partial_\nu\mathcal{R}_\rho+\partial_\mu\mathcal{R}_\nu\cdot\mathcal{R}_\rho)(U^\dagger\partial_\sigma U) \\
& -i(\partial_\mu\mathcal{L}_\nu\partial_\rho U\mathcal{R}_\sigma U^\dagger)+i(\partial_\mu\mathcal{R}_\nu\partial_\rho U^\dagger\mathcal{L}_\sigma U) \\
& -i\Big\{\mathcal{R}_\mu U^\dagger\mathcal{L}_\nu U(U^\dagger\partial_\rho U)(U^\dagger\partial_\sigma U)\Big\}+i\Big\{\mathcal{L}_\mu U\mathcal{R}_\nu U^\dagger(\partial_\rho U\cdot U^\dagger)(\partial_\sigma U\cdot U^\dagger)\Big\} \\
& -\frac{i}{2}\mathcal{L}_\mu(\partial_\nu U\cdot U^\dagger)\mathcal{L}_\rho(\partial_\sigma U\cdot U^\dagger)+\frac{i}{2}\mathcal{R}_\mu(U^\dagger\partial_\nu U)\mathcal{R}_\rho(U^\dagger\partial_\sigma U) \\
& +\mathcal{L}_\mu\mathcal{L}_\nu\mathcal{L}_\rho(\partial_\sigma U\cdot U^\dagger)+\mathcal{R}_\mu\mathcal{R}_\nu\mathcal{R}_\rho(U^\dagger\partial_\sigma U) \\
& +(\partial_\mu\mathcal{R}_\nu\cdot\mathcal{R}_\rho+\mathcal{R}_\mu\partial_\nu\mathcal{R}_\rho)U^\dagger\mathcal{L}_\sigma U-(\partial_\mu\mathcal{L}_\nu\cdot\mathcal{L}_\rho+\mathcal{L}_\mu\partial_\nu\mathcal{L}_\rho)U\mathcal{R}_\sigma U^\dagger \\
& +\mathcal{L}_\mu U\mathcal{R}_\nu U^\dagger\mathcal{L}_\rho(\partial_\sigma U\cdot U^\dagger)+\mathcal{R}_\mu U^\dagger\mathcal{L}_\nu U\mathcal{R}_\rho(U^\dagger\partial_\sigma U) \\
& -i\mathcal{R}_\mu\mathcal{R}_\nu\mathcal{R}_\rho U^\dagger\mathcal{L}_\sigma U+i\mathcal{L}_\mu\mathcal{L}_\nu\mathcal{L}_\rho U\mathcal{R}_\sigma U^\dagger-\frac{i}{2}U\mathcal{R}_\mu U^\dagger\mathcal{L}_\nu U\mathcal{R}_\rho U^\dagger\mathcal{L}_\sigma\Big], \qquad \text{(D.1)}
\end{aligned}
$$

with $N_c = 3$.

Appendix E

discretization for $x\partial_i\phi_a$

Here, we show the way of discretization for terms including a derivative as in Eq.(4.12). For instance, we first work on $x\partial_x\phi_3$:

$$[x\partial_x\phi_3]_{\rm disc} = \frac{[x\partial_x\bar{\phi}_3]_{\rm disc}}{\sqrt{\bar{\phi}_a\bar{\phi}_a}} - \frac{(\bar{\phi}_b[x\partial_x\bar{\phi}_b]_{\rm disc})\bar{\phi}_3}{(\bar{\phi}_a\bar{\phi}_a)^{3/2}}. \tag{E.1}$$

We make discretizations for the square bracket parts $[\ \ ]_{\rm disc}$. For $[x\partial_x\bar{\phi}_0]_{\rm disc}$, we have

$$\begin{aligned}
x\partial_x\bar{\phi}_0(x,y,z) &= x\partial_x\int_0^\infty\frac{dp_x}{(2\pi)}\int_0^\infty\frac{dp_y}{(2\pi)}\int_0^\infty\frac{dp_z}{(2\pi)}\bar{\phi}_0(\boldsymbol{p})8\cos(p_xx)\cos(p_yy)\cos(p_zz)\\
&= \int_0^\infty\frac{dp_x}{(2\pi)}\int_0^\infty\frac{dp_y}{(2\pi)}\int_0^\infty\frac{dp_z}{(2\pi)}\bar{\phi}_0(\boldsymbol{p})8\left[p_x\partial_{p_x}\cos(p_xx)\right]\cos(p_yy)\cos(p_zz)\\
&\xrightarrow{\text{discretization}} \sum_{a,b,c}\bar{\beta}_{abc}\frac{a\pi}{L}\frac{\cos\{(a+2)\pi x/L\}-\cos(a\pi x/L)}{2\pi/L}\cos(b\pi y/L)\cos(c\pi z/L)\\
&\equiv [x\partial_x\bar{\phi}_0]_{\rm disc}]_{\rm disc}(x,y,z)\,.
\end{aligned} \tag{E.2}$$

In a similar way, other terms read

$$\begin{aligned}
[x\partial_x\bar{\phi}_1]_{\rm disc} &= \sum_{h,k,l}\bar{\alpha}^{(1)}_{hkl}\frac{h\pi}{L}\frac{\sin\{(h+2)\pi x/L\}-\sin(h\pi x/L)}{2\pi/L}\cos(k\pi y/L)\cos(l\pi z/L)\,,\\
[x\partial_x\bar{\phi}_2]_{\rm disc} &= \sum_{h,k,l}\bar{\alpha}^{(2)}_{hkl}\frac{l\pi}{L}\frac{\cos\{(l+2)\pi x/L\}-\cos(l\pi x/L)}{2\pi/L}\sin(h\pi y/L)\cos(k\pi z/L)\,,\\
[x\partial_x\bar{\phi}_3]_{\rm disc} &= \sum_{h,k,l}\bar{\alpha}^{(3)}_{hkl}\frac{k\pi}{L}\frac{\cos\{(k+2)\pi x/L\}-\cos(k\pi x/L)}{2\pi/L}\cos(l\pi y/L)\sin(h\pi z/L)\,.
\end{aligned} \tag{E.3}$$

By putting those terms into the right-hand side of Eq.(E.1), the discretized form of $x\partial_x\phi_3$ is thus obtained.

Bibliography

[1] J. O. Andersen, W. R. Naylor and A. Tranberg, "Phase diagram of QCD in a magnetic field: A review," Rev. Mod. Phys. **88**, 025001 (2016) doi:10.1103/RevModPhys.88.025001 [arXiv:1411.7176 [hep-ph]].

[2] M. N. Chernodub, Phys. Rev. D **82**, 085011 (2010) doi:10.1103/PhysRevD.82.085011 [arXiv:1008.1055 [hep-ph]].

[3] N. Callebaut, D. Dudal and H. Verschelde, PoS FACESQCD , 046 (2010) [arXiv:1102.3103 [hep-ph]].

[4] M. Ammon, J. Erdmenger, P. Kerner and M. Strydom, Phys. Lett. B **706**, 94 (2014) doi:10.1016/j.physletb.2011.10.067 [arXiv:1106.4551 [hep-th]].

[5] M. Frasca, JHEP **1311**, 099 (2013) doi:10.1007/JHEP11(2013)099 [arXiv:1309.3966 [hep-ph]].

[6] H. Liu, L. Yu and M. Huang, Phys. Rev. D **91**, no. 1, 014017 (2015) doi:10.1103/PhysRevD.91.014017 [arXiv:1408.1318 [hep-ph]]; H. Liu, L. Yu and M. Huang, arXiv:1507.05809 [hep-ph].

[7] P. Filip, J. Phys. Conf. Ser. **636**, no. 1, 012013 (2015) doi:10.1088/1742-6596/636/1/012013 [arXiv:1504.07008 [hep-ph]].

[8] M. Kawaguchi and S. Matsuzaki, Phys. Rev. D **93**, no. 12, 125027 (2016) doi:10.1103/PhysRevD.93.125027 [arXiv:1511.06990 [hep-ph]].

[9] M. Bando, T. Kugo, S. Uehara, K. Yamawaki and T. Yanagida, Phys. Rev. Lett. **54**, 1215 (1985). doi:10.1103/PhysRevLett.54.1215

[10] M. Bando, T. Kugo and K. Yamawaki, Phys. Rept. **164**, 217 (1988). doi:10.1016/0370-1573(88)90019-1

[11] M. Kawaguchi and S. Matsuzaki, Eur. Phys. J. A **53**, no. 4, 68 (2017) doi:10.1140/epja/i2017-12254-1 [arXiv:1610.08942 [hep-ph]].

[12] A. Bandyopadhyay and S. Mallik, Eur. Phys. J. C **77**, no. 11, 771 (2017) doi:10.1140/epjc/s10052-017-5357-9 [arXiv:1610.07887 [hep-ph]].

[13] I. A. Shushpanov and A. V. Smilga, "Quark condensate in a magnetic field," Phys. Lett. B **402**, 351 (1997) doi:10.1016/S0370-2693(97)00441-3 [hep-ph/9703201].

[14] N. O. Agasian and I. A. Shushpanov, "Gell-Mann-Oakes-Renner relation in a magnetic field at finite temperature," JHEP **0110**, 006 (2001) doi:10.1088/1126-6708/2001/10/006 [hep-ph/0107128].

[15] E. S. Werbos, "The Chiral condensate in a constant electromagnetic field at O(p**6)," Phys. Rev. C **77**, 065202 (2008) doi:10.1103/PhysRevC.77.065202 [arXiv:0711.2635 [hep-ph]].

[16] J. O. Andersen, "Thermal pions in a magnetic background," Phys. Rev. D **86**, 025020 (2012) doi:10.1103/PhysRevD.86.025020 [arXiv:1202.2051 [hep-ph]].

[17] T. Inagaki, D. Kimura and T. Murata, "Four fermion interaction model in a constant magnetic field at finite temperature and chemical potential," Prog. Theor. Phys. **111**, 371 (2004) doi:10.1143/PTP.111.371 [hep-ph/0312005].

[18] D. P. Menezes, M. Benghi Pinto, S. S. Avancini, A. Perez Martinez and C. Providencia, "Quark matter under strong magnetic fields in the Nambu-Jona-Lasinio Model," Phys. Rev. C **79**, 035807 (2009) doi:10.1103/PhysRevC.79.035807 [arXiv:0811.3361 [nucl-th]].

[19] J. K. Boomsma and D. Boer, "The Influence of strong magnetic fields and instantons on the phase structure of the two-flavor NJL model," Phys. Rev. D **81**, 074005 (2010) doi:10.1103/PhysRevD.81.074005 [arXiv:0911.2164 [hep-ph]].

[20] L. Yu, J. Van Doorsselaere and M. Huang, "Inverse Magnetic Catalysis in the three-flavor NJL model with axial-vector interaction," Phys. Rev. D **91**, no. 7, 074011 (2015) doi:10.1103/PhysRevD.91.074011 [arXiv:1411.7552 [hep-ph]].

[21] H. Liu, X. Wang, L. Yu and M. Huang, "Neutral and charged (pseduo)scalar mesons and diquarks under magnetic fields," Phys. Rev. D **97**, no. 7, 076008 (2018) doi:10.1103/PhysRevD.97.076008 [arXiv:1801.02174 [hep-ph]].

[22] R. Derradi de Souza, T. Koide and T. Kodama, Prog. Part. Nucl. Phys. **86**, 35 (2016) doi:10.1016/j.ppnp.2015.09.002 [arXiv:1506.03863 [nucl-th]].

[23] D. Kharzeev and A. Zhitnitsky, Nucl. Phys. A **797**, 67 (2007) doi:10.1016/j.nuclphysa.2007.10.001.

[24] D. E. Kharzeev, L. D. McLerran and H. J. Warringa, Nucl. Phys. A **803**, 227 (2008) doi:10.1016/j.nuclphysa.2008.02.298.

[25] K. Fukushima, D. E. Kharzeev and H. J. Warringa, Phys. Rev. D **78**, 074033 (2008) doi:10.1103/PhysRevD.78.074033.

[26] A. A. Andrianov, V. A. Andrianov, D. Espriu and X. Planells, Phys. Lett. B **710**, 230 (2012) doi:10.1016/j.physletb.2012.02.072.

[27] A. A. Andrianov, D. Espriu and X. Planells, Eur. Phys. J. C **73**, no. 1, 2294 (2013) doi:10.1140/epjc/s10052-013-2294-0.

[28] M. Kawaguchi, M. Harada, S. Matsuzaki and R. Ouyang, Phys. Rev. C **95**, no. 6, 065204 (2017) doi:10.1103/PhysRevC.95.065204 [arXiv:1612.00616 [nucl-th]].

[29] T. H. R. Skyrme, Nucl. Phys. **31**, 556 (1962). doi:10.1016/0029-5582(62)90775-7

[30] E. Witten, Nucl. Phys. B **223**, 422 (1983). doi:10.1016/0550-3213(83)90063-9

[31] E. Witten, Nucl. Phys. B **223**, 433 (1983). doi:10.1016/0550-3213(83)90064-0

[32] I. R. Klebanov, "Nuclear Matter in the Skyrme Model," Nucl. Phys. B **262**, 133 (1985). doi:10.1016/0550-3213(85)90068-9

[33] H. J. Lee, B. Y. Park, D. P. Min, M. Rho and V. Vento, Nucl. Phys. A **723**, 427 (2003) doi:10.1016/S0375-9474(03)01452-0 [hep-ph/0302019].

[34] H. J. Lee, B. Y. Park, M. Rho and V. Vento, "The Pion velocity in dense skyrmion matter," Nucl. Phys. A **741**, 161 (2004) doi:10.1016/j.nuclphysa.2004.06.010 [hep-ph/0307111].

[35] Y. L. Ma, M. Harada, H. K. Lee, Y. Oh, B. Y. Park and M. Rho, "Dense baryonic matter in the hidden local symmetry approach: Half-skyrmions and nucleon mass," Phys. Rev. D **88**, no. 1, 014016 (2013) Erratum: [Phys. Rev. D **88**, no. 7, 079904 (2013)] doi:10.1103/PhysRevD.88.014016, 10.1103/PhysRevD.88.079904 [arXiv:1304.5638 [hep-ph]].

[36] Y. L. Ma, M. Harada, H. K. Lee, Y. Oh, B. Y. Park and M. Rho, "Dense baryonic matter in conformally-compensated hidden local symmetry: Vector manifestation and chiral symmetry restoration," Phys. Rev. D **90**, no. 3, 034015 (2014) doi:10.1103/PhysRevD.90.034015 [arXiv:1308.6476 [hep-ph]].

[37] Y. L. Ma and M. Rho, "Recent progress on dense nuclear matter in skyrmion approaches," Sci. China Phys. Mech. Astron. **60**, no. 3, 032001 (2017) doi:10.1007/s11433-016-0497-2 [arXiv:1612.06600 [nucl-th]].

[38] J. S. Schwinger, Annals Phys. **2**, 407 (1957). doi:10.1016/0003-4916(57)90015-5

[39] M. Gell-Mann and M. Levy, Nuovo Cim. **16**, 705 (1960). doi:10.1007/BF02859738

[40] G. Holzwarth and B. Schwesinger, Rept. Prog. Phys. **49**, 825 (1986). doi:10.1088/0034-4885/49/8/001

[41] I. Zahed and G. E. Brown, Phys. Rept. **142**, 1 (1986). doi:10.1016/0370-1573(86)90142-0

[42] Y. L. Ma and M. Harada, arXiv:1604.04850 [hep-ph].

[43] C. Patrignani *et al.* [Particle Data Group], Chin. Phys. C **40**, no. 10, 100001 (2016). doi:10.1088/1674-1137/40/10/100001

[44] B. R. He, Phys. Rev. D **92**, no. 11, 111503 (2015) doi:10.1103/PhysRevD.92.111503 [arXiv:1510.04683 [hep-ph]].

[45] M. Harada, H. K. Lee, Y. L. Ma and M. Rho, Phys. Rev. D **91**, no. 9, 096011 (2015) doi:10.1103/PhysRevD.91.096011 [arXiv:1502.02508 [hep-ph]].

[46] K. Nishiyama, S. Karasawa and T. Tatsumi, Phys. Rev. D **92**, 036008 (2015) doi:10.1103/PhysRevD.92.036008 [arXiv:1505.01928 [nucl-th]].

[47] M. Buballa and S. Carignano, Eur. Phys. J. A **52**, no. 3, 57 (2016) doi:10.1140/epja/i2016-16057-6 [arXiv:1508.04361 [nucl-th]].

[48] H. Abuki, EPJ Web Conf. **129**, 00036 (2016) doi:10.1051/epjconf/201612900036 [arXiv:1609.04605 [hep-ph]].

[49] H. Abuki, JPS Conf. Proc. **20**, 011017 (2018). doi:10.7566/JPSCP.20.011017

[50] A. S. Goldhaber and N. S. Manton, "Maximal Symmetry of the Skyrme Crystal," Phys. Lett. B **198**, 231 (1987). doi:10.1016/0370-2693(87)91502-4

[51] V. P. Gusynin, V. A. Miransky and I. A. Shovkovy, "Dimensional reduction and catalysis of dynamical symmetry breaking by a magnetic field," Nucl. Phys. B **462**, 249 (1996) doi:10.1016/0550-3213(96)00021-1 [hep-ph/9509320].

[52] D. T. Son and M. A. Stephanov, "Axial anomaly and magnetism of nuclear and quark matter," Phys. Rev. D **77**, 014021 (2008).

[53] M. Eto, K. Hashimoto and T. Hatsuda, "Ferromagnetic neutron stars: axial anomaly, dense neutron matter, and pionic wall," Phys. Rev. D **88**, 081701 (2013) .

[54] W. G. Paeng, T. T. S. Kuo, H. K. Lee, Y. L. Ma and M. Rho, "Scale-invariant hidden local symmetry, topology change, and dense baryonic matter. II.," Phys. Rev. D **96**, no. 1, 014031 (2017).

[55] Y. L. Li, Y. L. Ma and M. Rho, "The Non-Quenching of g_A in Nuclei and Emergent Scale Symmetry in Dense Baryonic Matter," arXiv:1804.00310 [nucl-th].

[56] Y. L. Ma, H. K. Lee, W. G. Paeng and M. Rho, "A pseudo-conformal equation of state in compact-star matter from topology change and hidden symmetries of QCD," arXiv:1804.00305 [nucl-th].

[57] I.E. Dzyaloshinsky, Theory of helicoidal structures in antiferromagnets. I. Nonmetals. Sov. Phys. JETP 19 (1964) 960.

[58] Y Togawa. 2012. Chiral magnetic soliton lattice on a chiral helimagnet hRvL.108j7202T Y. Togawa et al Chiral magnetic soliton lattice on a chiral helimagnet. Phys.Rev.Lett.,108,107202

[59] T. Hatsuda, Prog. Theor. Phys. **75**, 301 (1986) Erratum: [Prog. Theor. Phys. **75**, 996 (1986)]. doi:10.1143/PTP.75.301

[60] T. Brauner and N. Yamamoto, JHEP **1704**, 132 (2017) doi:10.1007/JHEP04(2017)132 [arXiv:1609.05213 [hep-ph]].

[61] M. Kawaguchi, Y. L. Ma and S. Matsuzaki, arXiv:1810.12880 [nucl-th].

[62] G. 't Hooft, Nucl. Phys. B **72**, 461 (1974). doi:10.1016/0550-3213(74)90154-0

[63] O. Kaymakcalan, S. Rajeev and J. Schechter, Phys. Rev. D **30**, 594 (1984). doi:10.1103/PhysRevD.30.594

[64] T. Fujiwara, T. Kugo, H. Terao, S. Uehara and K. Yamawaki, Prog. Theor. Phys. **73**, 926 (1985). doi:10.1143/PTP.73.926